J|A|C|S
ARTICLES
Published on Web 08/24/2006

Pentacyanoiron(II) as an Electron Donor Group for Nonlinear Optics: Medium-Responsive Properties and Comparisons with Related Pentaammineruthenium(II) Complexes

Benjamin J. Coe,*[,†] Josephine L. Harries,[†] Madeleine Helliwell,[†] Lathe A. Jones,[†] Inge Asselberghs,[‡] Koen Clays,[‡] Bruce S. Brunschwig,[§] James A. Harris,[§] Javier Garín,[||] and Jesús Orduna[||]

Contribution from the School of Chemistry, University of Manchester, Oxford Road, Manchester M13 9PL, U.K., Department of Chemistry, University of Leuven, Celestijnenlaan 200D, B-3001 Leuven, Belgium, Molecular Materials Research Center, Beckman Institute, MC 139-74, California Institute of Technology, 1200 East California Boulevard, Pasadena, California 91125, and Departamento de Química Orgánica, ICMA, Universidad de Zaragoza-CSIC, E-50009 Zaragoza, Spain

Received May 17, 2006; E-mail: b.coe@man.ac.uk.

Abstract: In this article, we describe a series of complex salts in which electron-rich $\{Fe^{II}(CN)_5\}^{3-}$ centers are coordinated to pyridyl ligands with electron-accepting *N*-methyl/aryl-pyridinium substituents. These compounds have been characterized by using various techniques including electronic absorption spectroscopy and cyclic voltammetry. Molecular quadratic nonlinear optical (NLO) responses have been determined by using hyper-Rayleigh scattering (HRS) at 1064 nm, and also via Stark (electroabsorption) spectroscopic studies on the intense, visible $d \rightarrow \pi^*$ metal-to-ligand charge-transfer (MLCT) bands. The relatively large static first hyperpolarizabilities, β_0, increase markedly on moving from aqueous to methanol solutions, accompanied by large red-shifts in the MLCT transitions. Acidification of aqueous solutions allows reversible switching of the linear and NLO properties, as shown via both HRS and Stark experiments. Time-dependent density functional theory and finite field calculations using a polarizable continuum model yield relatively good agreement with the experimental results and confirm the large decrease in β_0 on protonation. The Stark-derived β_0 values are generally larger for related $\{Ru^{II}(NH_3)_5\}^{2+}$ complexes than for their $\{Fe^{II}(CN)_5\}^{3-}$ analogues, consistent with the HRS data in water. However, the HRS data in methanol show that the stronger solvatochromism of the Fe^{II} complexes causes their NLO responses to surpass those of their Ru^{II} counterparts upon changing the solvent medium.

Introduction

The need for new designer materials for potential uses in sophisticated optical data processing devices has stimulated much interest in organic compounds that display nonlinear optical (NLO) behavior.[1] Quadratic (second-order) NLO effects are amenable to opto-electronic applications, while cubic (third-order) phenomena are suited to all-optical technologies. A diverse range of chromophores are known to display very large molecular NLO responses, as characterized by first and second hyperpolarizabilities (β and γ) from which originate quadratic and cubic effects, respectively. As a subclass of molecular NLO compounds, transition metal complexes are especially interesting because they can combine all of the attractive features of organic species with added multifunctionality.[2] Noteworthy examples illustrating the promise of metal complexes in this field are provided by a number of demonstrations of the use of metal-based redox to switch both quadratic and cubic NLO responses.[3]

Large values of β are typically displayed by molecules that incorporate charge asymmetry into an extended π-conjugated

[†] University of Manchester.
[‡] University of Leuven.
[§] California Institute of Technology.
[||] Universidad de Zaragoza.

(1) (a) Zyss, J. *Molecular Nonlinear Optics: Materials, Physics and Devices*; Academic Press: Boston, 1994. (b) Bosshard, Ch., Sutter, K., Prêtre, Ph., Hulliger, J., Flörsheimer, M., Kaatz, P., Günter, P. *Organic Nonlinear Optical Materials (Advances in Nonlinear Optics, Vol. 1.)*; Gordon and Breach: Amsterdam, The Netherlands, 1995. (c) *Nonlinear Optics of Organic Molecules and Polymers*; Nalwa, H. S., Miyata, S., Eds.; CRC Press: Boca Raton, FL, 1997. (d) Marder, S. R. *Chem. Commun.* **2006**, 131−134. (e) *Nonlinear Optical Properties of Matter: From Molecules to Condensed Phases*; Papadopoulos, M. G., Leszczynski, J., Sadlej, A. J., Eds.; Kluwer: Dordrecht, 2006.

(2) (a) Kanis, D. R.; Ratner, M. A.; Marks, T. J. *Chem. Rev.* **1994**, *94*, 195−242. (b) Long, N. J. *Angew. Chem., Int. Ed. Engl.* **1995**, *34*, 21−38. (c) Whittall, I. R.; McDonagh, A. M.; Humphrey, M. G.; Samoc, M. *Adv. Organomet. Chem.* **1998**, *42*, 291−362. (d) Whittall, I. R.; McDonagh, A. M.; Humphrey, M. G.; Samoc, M. *Adv. Organomet. Chem.* **1998**, *43*, 349−405. (e) Heck, J.; Dabek, S.; Meyer-Friedrichsen, T.; Wong, H. *Coord. Chem. Rev.* **1999**, *190−192*, 1217−1254. (f) Gray, G. M.; Lawson, C. M. In *Optoelectronic Properties of Inorganic Compounds*; Roundhill, D. M.; Fackler, J. P., Jr., Eds.; Plenum: New York, U.S.A., 1999; pp 1−27. (g) Shi, S. In *Optoelectronic Properties of Inorganic Compounds*; Roundhill, D. M.; Fackler, J. P., Jr., Eds.; Plenum: New York, U.S.A., 1999; pp 55−105. (h) Le Bozec, H.; Renouard, T. *Eur. J. Inorg. Chem.* **2000**, 229−239. (i) Barlow, S.; Marder, S. R. *Chem. Commun.* **2000**, 1555−1562. (j) Lacroix, P. G. *Eur. J. Inorg. Chem.* **2001**, 339−348. (k) Di Bella, S. *Chem. Soc. Rev.* **2001**, *30*, 355−366. (l) Coe, B. J. In *Comprehensive Coordination Chemistry II*; McCleverty, J. A., Meyer, T. J., Eds.; Elsevier Pergamon: Oxford, U.K., 2004; Vol. 9, pp 621−687. (m) Coe, B. J. *Acc. Chem. Res.* **2006**, *39*, 383−393.

10.1021/ja063449m CCC: $33.50

system, and such chromophores also exhibit intramolecular charge-transfer transitions. Experimentally measured β values are therefore enhanced to variable degrees by resonance, and it is necessary to derive static (off-resonance) first hyperpolarizabilities, β_0, in order to derive meaningful molecular structure−activity relationships. In addition, since practical applications must avoid any actual absorption of light, β_0 values are the most relevant parameter used to characterize new chromophores. The great majority of metal-containing NLO chromophores contain electron-rich metal center(s), so their β responses are associated with metal-to-ligand charge-transfer (MLCT) transitions.

Our previous contributions to the field of organotransition metal NLO compounds have focused primarily on the quadratic NLO properties of a range of ruthenium ammine complexes of pyridinium-substituted ligands.[2m,3a,4] Recently, we have also been extending our scope to include other types of complexes, and one promising, readily accessible, and suitably electron-rich metal center is $\{Fe^{II}(CN)_5\}^{3-}$. Many previous reports have described the syntheses and properties of complexes containing this moiety coordinated to a wide variety of ligands,[5] including many discussions of MLCT spectroscopic properties, but no NLO studies with such complexes have hitherto been disclosed. Of particular relevance to our investigations, the complex $[Fe^{II}(CN)_5(MeQ^+)]^{2-}$ (MeQ^+ = *N*-methyl-4,4′-bipyridinium) was first reported by Toma and Malin,[5a] but only very limited characterization data were presented at the time (i.e., UV−vis absorption data). Subsequent studies with this particular complex have included ^{13}C NMR spectroscopy,[6] photochemical ligand loss,[5b] outer-sphere complexation,[7] cyclic voltammetric data,[5d,8] formation kinetics,[9] and the effects of inclusion into a cyclodextrin cavity.[10] The outer-sphere complexation properties and formation kinetics of the closely related complex $[Fe^{II}(CN)_5(Mebpe^+)]^{2-}$ ($Mebpe^+$ = *N*-methyl-4-[*trans*-2-(4-pyridyl)ethenyl]pyridinium) have also been investigated.[7,9] In the present study, we have prepared a series of complex salts $Na_2[Fe^{II}(CN)_5L]$ (where L is MeQ^+, $Mebpe^+$, or a related pyridyl pyridinium ligand) and investigated their electronic and optical properties by using a range of techniques. The results obtained allow us to make detailed comparisons between the new compounds and related complex salts containing $\{Ru^{II}(NH_3)_5\}^{2+}$ electron-donor groups and also to demonstrate a novel chemical approach to switching of molecular NLO responses.

Experimental Section

Materials and Procedures. The compound $Na_3[Fe^{II}(CN)_5(NH_3)]$ was obtained from Aldrich and purified by recrystallization before use. The pro-ligand salts *N*-methyl-4,4′-bipyridinium chloride ($[MeQ^+]Cl\cdot 0.7H_2O$),[4c] *N*-phenyl-4,4′-bipyridinium chloride ($[PhQ^+]Cl\cdot 2H_2O$),[11] *N*-(4-acetylphenyl)-4,4′-bipyridinium chloride ($[4\text{-}AcPhQ^+]Cl\cdot 2H_2O$),[11] *N*-(2-pyrimidyl)-4,4′-bipyridinium chloride ($[2\text{-}PymQ^+]Cl$),[12] and *N*-methyl-4-[*trans*-2-(4-pyridyl)ethenyl]pyridinium iodide ($[Mebpe^+]I$)[13] and the compound 4-methyl-*N*-phenylpyridinium chloride $[Phpic^+]Cl$[12] were synthesized according to published methods. We have previously reported preparations of the intermediate compounds *N*-(2,4-dinitrophenyl)-4,4′-bipyridinium chloride ($[2,4\text{-}DNPhQ^+]Cl$)[11] and *N*-phenyl-4-[*trans*-2-(4-pyridyl)ethenyl]pyridinium chloride ($[Phbpe^+]Cl\cdot 2.25H_2O$),[12] but considerably improved methods are included here. The complex salts $[Ru^{II}(NH_3)_5(MeQ^+)]Cl_3$, $[Ru^{II}(NH_3)_5(PhQ^+)]Cl_3$, and $[Ru^{II}(NH_3)_5(4\text{-}AcPhQ^+)]Cl_3$ were prepared as previously described,[3a] and the analogous compounds containing $2\text{-}PymQ^+$, $Mebpe^+$, or $Phbpe^+$ ligands were prepared from their hexafluorophosphate counterparts by precipitation from acetone/LiCl. All other reagents were obtained commercially and used as supplied. All solvents were degassed by argon purging for 10 min prior to use, and all reactions were conducted under an argon atmosphere in the dark. Products were dried at room temperature in a vacuum desiccator ($CaSO_4$) for ca. 24 h prior to characterization.

General Physical Measurements. ^1H NMR spectra were recorded on a Varian Gemini 200 spectrometer, and all shifts are referenced to TMS. The fine splitting of pyridyl or phenyl ring AA′BB′ patterns is ignored, and the signals are reported as simple doublets, with *J* values referring to the two most intense peaks. Elemental and thermogravimetric analyses (TGA) were performed by the Microanalytical Laboratory, University of Manchester (TGA under N_2, heating to 250 °C). IR spectra were obtained as KBr disks with an ATI Mattson Genesis Series FTIR instrument, and UV−vis spectra were recorded by using a Hewlett-Packard 8452A diode array spectrophotometer, except for those presented in Table 2, which were measured using an α-Helios double-beam spectrophotometer that has a range further into the NIR region.

Cyclic voltammetric measurements were carried out with an EG&G PAR model 283 potentiostat/galvanostat. An EG&G PAR K0264 single-compartment microcell was used with a silver/silver chloride reference

(3) (a) Coe, B. J.; Houbrechts, S.; Asselberghs, I.; Persoons, A. *Angew. Chem., Int. Ed.* **1999**, *38*, 366−369. (b) Weyland, T.; Ledoux, I.; Brasselet, S.; Zyss, J.; Lapinte, C. *Organometallics* **2000**, *19*, 5235−5237. (c) Malaun, M.; Reeves, Z. R.; Paul, R. L.; Jeffery, J. C.; McCleverty, J. A.; Ward, M. D.; Asselberghs, I.; Clays, K.; Persoons, A. *Chem. Commun*. **2001**, 49−50. (d) Malaun, M.; et al., *J. Chem. Soc., Dalton Trans.* **2001**, 3025−3038. (e) Cifuentes, M. P.; Powell, C. E.; Humphrey, M. G.; Heath, G. A.; Samoc, M.; Luther-Davies, B. *J. Phys. Chem. A* **2001**, *105*, 9625−9627. (f) Paul, F.; Costuas, K.; Ledoux, I.; Deveau, S.; Zyss, J.; Halet, J.-F.; Lapinte, C. *Organometallics* **2002**, *21*, 5229−5235. (g) Powell, C. E.; Cifuentes, M. P.; Morrall, J. P.; Stranger, R.; Humphrey, M. G.; Samoc, M.; Luther-Davies, B.; Heath, G. A. *J. Am. Chem. Soc*. **2003**, *125*, 602−610. (h) Asselberghs, I.; Clays, K.; Persoons, A.; McDonagh, A. M.; Ward, M. D.; McCleverty, J. A. *Chem. Phys. Lett.* **2003**, *368*, 408−411. (i) Powell, C. E.; Humphrey, M. G.; Cifuentes, M. P.; Morrall, J. P.; Samoc, M.; Luther-Davies, B. *J. Phys. Chem. A* **2003**, *107*, 11264−11266. (j) Sporer, C. et al., *Angew. Chem., Int. Ed.* **2004**, *43*, 5266−5268.

(4) Selected recent examples: (a) Coe, B. J.; Jones, L. A.; Harris, J. A.; Sanderson, E. E.; Brunschwig, B. S.; Asselberghs, I.; Clays, K.; Persoons, A. *Dalton Trans*. **2003**, 2335−2341. (b) Coe, B. J.; Jones, L. A.; Harris, J. A.; Brunschwig, B. S.; Asselberghs, I.; Clays, K.; Persoons, A. *J. Am. Chem. Soc.* **2003**, *125*, 862−863. (c) Coe, B. J.; Jones, L. A.; Harris, J. A.; Brunschwig, B. S.; Asselberghs, I.; Clays, K.; Persoons, A.; Garín, J.; Orduna, J. *J. Am. Chem. Soc*. **2004**, *126*, 3880−3891. (d) Coe, B. J.; Harris, J. A.; Jones, L. A.; Brunschwig, B. S.; Song, K.; Clays, K.; Garín, J.; Orduna, J.; Coles, S. J.; Hursthouse, M. B. *J. Am. Chem. Soc.* **2005**, *127*, 4845−4859. (e) Coe, B. J.; Harries, J. L.; Helliwell, M.; Brunschwig, B. S.; Harris, J. A.; Asselberghs, I.; Hung, S.-T.; Clays, K.; Horton, P. N.; Hursthouse, M. B. *Inorg. Chem.* **2006**, *45*, 1215−1227.

(5) Selected examples: (a) Toma, H. E.; Malin, J. M. *Inorg. Chem.* **1973**, *12*, 1039−1045. (b) Figard, J. E.; Petersen, J. D. *Inorg. Chem.* **1978**, *17*, 1059−1063. (c) Hrepic, N. V.; Malin, J. M. *Inorg. Chem.* **1979**, *18*, 409−413. (d) Moore, K. J.; Lee, L.-S.; Mabbott, G. A.; Petersen, J. D. *Inorg. Chem.* **1983**, *22*, 1108−1112. (e) Johnson, C. R.; Shepherd, R. E. *Inorg. Chem.* **1983**, *22*, 1117−1123. (f) Johnson, C. R.; Shepherd, R. E. *Inorg. Chem.* **1983**, *22*, 2439−2444. (g) Macartney, D. H. *Rev. Inorg. Chem.* **1988**, *9*, 101−151. (h) Benedix, R.; Hennig, H. *Z. Anorg. Allg. Chem.* **1989**, *577*, 23−38. (i) Estrin, D. A.; Hamra, O. Y.; Paglieri, L.; Slep, L. D.; Olabe, J. A. *Inorg. Chem.* **1996**, *35*, 6832−6837. (j) Waldhör, E.; Kaim, W.; Olabe, J. A.; Slep, L. D.; Fiedler, J. *Inorg. Chem.* **1997**, *36*, 2969−2974. (k) Slep, L. D.; Pollak, S.; Olabe, J. A. *Inorg. Chem.* **1999**, *38*, 4369−4371. (l) Parise, A. R.; Piro, O. E.; Castellano, E. E.; Olabe, J. A. *Inorg. Chim. Acta* **2001**, *319*, 199−202. (m) Baraldo, L. M.; Forlano, P.; Parise, A. R.; Slep, L. D.; Olabe, J. A. *Coord. Chem. Rev.* **2001**, *219*−*221*, 881−921. (n) Alborés, P.; Slep, L. D.; Weyhermüller, T.; Baraldo, L. M. *Inorg. Chem.* **2004**, *43*, 6762−6773.

(6) Figard, J. E.; Paukstelis, J. V.; Byrne, E. F.; Petersen, J. D. *J. Am. Chem. Soc.* **1977**, *99*, 8417−8425.

(7) Toma, H. E. *Can. J. Chem.* **1979**, *57*, 2079−2084.

(8) Slep, L. D.; Baraldo, L. M.; Olabe, J. A. *Inorg. Chem.* **1996**, *35*, 6327−6333.

(9) Macartney, D. H.; Warrack, L. J. *Can. J. Chem.* **1989**, *67*, 1774−1779.

(10) Ando, I.; Ujimoto, K.; Kurihara, H. *Bull. Chem. Soc. Jpn.* **2001**, *74*, 717−721.

(11) Coe, B. J.; Harris, J. A.; Harrington, L. J.; Jeffery, J. C.; Rees, L. H.; Houbrechts, S.; Persoons, A. *Inorg. Chem.* **1998**, *37*, 3391−3399.

(12) Coe, B. J.; Harris, J. A.; Asselberghs, I.; Persoons, A.; Jeffery, J. C.; Rees, L. H.; Gelbrich, T.; Hursthouse, M. B. *J. Chem. Soc., Dalton Trans*. **1999**, 3617−3625.

(13) Bergman, E. D.; Crane, F. E., Jr.; Fuoss, R. M. *J. Am. Chem. Soc.* **1952**, *74*, 5979−5982.

electrode separated by a salt bridge from a glassy carbon disk working electrode and Pt wire auxiliary electrode. Water and methanol were distilled before use. KNO_3 and $[NBu^n_4]PF_6$, the latter twice recrystallized from ethanol and dried in vacuo, were used as supporting electrolytes. Solutions containing ca. 10^{-3} M analyte (0.1 M electrolyte) were deaerated by purging with N_2. All $E_{1/2}$ values were calculated from $(E_{pa} + E_{pc})/2$ at a scan rate of 200 mV s^{-1}.

Purification of $Na_3[Fe^{II}(CN)_5(NH_3)]$. Commercial $Na_3[Fe^{II}(CN)_5(NH_3)]$ (5.00 g) was heated to reflux in aqueous ammonia solution (100 mL, 70%). After 10 min under reflux, the solution was filtered while hot to remove a dark impurity. After the solution was cooled to room temperature, ethanol (100 mL) was added slowly with stirring. The precipitate was filtered off, washed with ethanol then diethyl ether, and dried to afford a light yellow solid (4.70 g).

Improved Synthesis of *N*-(2,4-Dinitrophenyl)-4,4′-bipyridinium Chloride, [2,4-DNPhQ$^+$]Cl. A solution of 2,4-dinitrochlorobenzene (6.49 g, 32 mmol) and 4,4′-bipyridyl (5.00 g, 32 mmol) in ethanol (50 mL) was heated under reflux for 23 h. The solution was cooled to room temperature and added to diethyl ether (500 mL), with stirring. The golden-brown precipitate was filtered off and washed with diethyl ether: 9.46 g, 82%; δ_H (D_2O) 9.38 (1 H, d, J = 2.4 Hz, H^3), 9.23 (2 H, d, J = 6.9 Hz, C_5H_4N-Ph), 8.92 (1 H, dd, J = 8.7, 2.5 Hz, H^5), 8.82 (2 H, d, J = 6.3 Hz, C_5H_4N), 8.68 (2 H, d, J = 6.8 Hz, C_5H_4N-Ph), 8.25 (1 H, d, J = 8.6 Hz, H^6), 8.01 (2 H, d, J = 6.3 Hz, C_5H_4N). Note: The product is hygroscopic and prolonged contact with air causes formation of a sticky brown solid.

Improved Synthesis of *N*-Phenyl-4-[*E*-2-(4-pyridyl)ethenyl]pyridinium Chloride, [Phbpe$^+$]Cl. To a solution of [Phpic$^+$]Cl (100 mg, 0.48 mmol) and pyridine-4-carboxaldehyde (0.05 mL, 0.45 mmol) in ethanol (ca. 0.5 mL) was added 1 drop of pyridine. The solution was heated at 95 °C for 3.5 h. The resulting dark brown solution was cooled to room temperature, and the product precipitated by the dropwise addition of diethyl ether. A dark brown solid was filtered off and washed with diethyl ether: 119 mg, 84%; δ_H (D_2O) 8.94 (2 H, d, J = 6.7 Hz, C_5H_4N), 8.51 (2 H, d, J = 6.0 Hz, C_5H_4N), 8.21 (2 H, d, J = 6.9 Hz, C_5H_4N), 7.75 (1 H, d, J = 16.2 Hz, CH), 7.69 (5 H, s, Ph), 7.63 (2 H, d, J = 6.1 Hz, C_5H_4N), 7.56 (1 H, d, J = 16.4 Hz, CH). Anal. Calcd (%) for $C_{18}H_{15}ClN_2\cdot 2.75H_2O$: C, 62.79; H, 6.00; N, 8.14. Found: C, 63.17; H, 5.74; N, 7.95.

Synthesis of $Na_2[Fe^{II}(CN)_5(MeQ^+)]$, 1. A solution of $Na_3[Fe^{II}(CN)_5(NH_3)]$ (136 mg, 0.500 mmol) and $[MeQ^+]Cl\cdot 0.7H_2O$ (103 mg, 0.470 mmol) in water (5 mL) was stirred at room temperature for 6 h in the dark. Ethanol (30 mL) was added, and the mixture stored at 4 °C in a refrigerator overnight. The purple-blue solid was filtered off and washed with ethanol. The product was purified by three reprecipitations from water/ethanol to afford a dark purple-blue solid: 164 mg, 72%; δ_H (D_2O) 9.15 (2 H, d, J = 6.7 Hz, C_5H_4N), 8.80 (2 H, d, J = 6.7 Hz, C_5H_4N), 8.17 (2 H, d, J = 6.7 Hz, C_5H_4N), 7.48 (2 H, d, J = 6.9 Hz, C_5H_4N), 4.41 (3H, s, Me). ν(C≡N) 2080w, 2048m, 2042s cm^{-1}. Anal. Calcd (%) for $C_{16}H_{11}N_7FeNa_2\cdot 4.5H_2O$: C, 39.69; H, 4.16; N, 20.25. Found: C, 39.87; H, 3.70; N, 20.14. TGA analysis indicates the loss of ca. 4.1 molecules of water upon heating.

Synthesis of $Na_2[Fe^{II}(CN)_5(PhQ^+)]$, 2. This compound was prepared and purified in manner similar to **1** by using $[PhQ^+]Cl\cdot 2H_2O$ (134 mg, 0.440 mmol) in place of $[MeQ^+]Cl\cdot 0.7H_2O$ to afford a dark blue solid: 170 mg, 65%; δ_H (D_2O) 9.18 (2 H, d, J = 6.6 Hz, C_5H_4N), 9.14 (2 H, d, J = 6.9 Hz, C_5H_4N), 8.48 (2 H, d, J = 6.6 Hz, C_5H_4N), 7.73 (5 H, m, Ph), 7.62 (2 H, d, J = 6.3 Hz, C_5H_4N). ν(C≡N) 2100w, 2080m, 2048s cm^{-1}. Anal. Calcd (%) for $C_{21}H_{13}N_7FeNa_2\cdot 7H_2O$: C, 42.66; H, 4.60; N, 16.58. Found: C, 42.28; H, 4.18; N, 16.92. TGA analysis indicates the loss of ca. 6.2 molecules of water upon heating.

Synthesis of $Na_2[Fe^{II}(CN)_5(4\text{-}AcPhQ^+)]$, 3. This compound was prepared and purified in manner similar to **1** by using $[4\text{-}AcPhQ^+]Cl\cdot 2H_2O$ (155 mg, 0.447 mmol) in place of $[MeQ^+]Cl\cdot 0.7H_2O$ to afford a dark blue solid: 200 mg, 69%; δ_H (D_2O) 9.25 (2 H, d, J = 6.3 Hz, C_5H_4N), 9.16 (2 H, d, J = 5.9 Hz, C_5H_4N), 8.50 (2 H, d, J = 5.7 Hz, C_5H_4N), 8.23 (2 H, d, J = 8.3 Hz, C_6H_4), 7.95 (2 H, d, J = 8.2 Hz, C_6H_4), 7.61 (2 H, d, J = 6.4 Hz, C_5H_4N), 2.72 (3 H, s, Me). ν(C≡N) 2110w, 2084m, 2048s cm^{-1}. Anal. Calcd (%) for $C_{23}H_{15}N_7FeNa_2O\cdot 8H_2O$: C, 42.41; H, 4.80; N, 15.05. Found: C, 42.16; H, 4.15; N, 15.56. TGA analysis indicates the loss of ca. 7.3 molecules of water upon heating.

Synthesis of $Na_2[Fe^{II}(CN)_5(2\text{-}PymQ^+)]$, 4. This compound was prepared and purified in manner similar to **1** by using $[2\text{-}PymQ^+]Cl$ (135 mg, 0.499 mmol) in place of $[MeQ^+]Cl\cdot 0.7H_2O$ to afford a dark blue/green solid: 120 mg, 39%; δ_H (D_2O) 10.01 (2 H, d, J = 6.6 Hz, C_5H_4N), 9.24 (2 H, d, J = 6.0 Hz, C_5H_4N), 9.06 (2 H, d, J = 4.8 Hz, $C_4H_3N_2$), 8.57 (2 H, d, J = 6.9 Hz, C_5H_4N), 7.90 (1 H, t, J = 11.2 Hz, $C_4H_3N_2$), 7.66 (2 H, d, J = 6.4 Hz, C_5H_4N). ν(C≡N) 2119w, 2086m, 2050s cm^{-1}. Anal. Calcd (%) for $C_{19}H_{11}N_9FeNa_2\cdot 8.5H_2O$: C, 36.79; H, 4.55; N, 20.32. Found: C, 36.38; H, 3.73; N, 20.95. TGA analysis indicates the loss of ca. 7.0 molecules of water upon heating.

Synthesis of $Na_2[Fe^{II}(CN)_5(Mebpe^+)]$, 5. This compound was prepared and purified in manner similar to **1** by using $[Mebpe^+]I$ (162 mg, 0.500 mmol) in place of $[MeQ^+]Cl\cdot 0.7H_2O$ to afford a dark purple-blue solid: 82 mg, 29%; δ_H (D_2O) 8.86 (2 H, d, J = 6.6 Hz, C_5H_4N), 8.48 (2 H, d, J = 6.6 Hz, C_5H_4N), 7.73 (2 H, d, J = 6.9 Hz, C_5H_4N), 7.36−7.17 (2 H, m, 2CH), 7.01 (2 H, d, J = 6.9 Hz, C_5H_4N), 4.24 (3 H, s, Me). ν(C≡N) 2086w, 2044s cm^{-1}. Anal. Calcd (%) for $C_{18}H_{13}N_7FeNa_2\cdot 7.5H_2O$: C, 38.31; H, 5.00; N, 17.38. Found: C, 37.82; H, 4.37; N, 17.03. TGA analysis indicates the loss of ca. 7.6 molecules of water upon heating.

Synthesis of $Na_2[Fe^{II}(CN)_5(Phbpe^+)]$, 6. This compound was prepared and purified in manner similar to **1** by using $[Phbpe^+]Cl\cdot 2.25H_2O$ (146 mg, 0.435 mmol) in place of $[MeQ^+]Cl\cdot 0.7H_2O$ to afford a dark blue solid: 161 mg, 66%; δ_H (D_2O) 8.93 (4 H, m, C_5H_4N), 8.10 (2 H, d, J = 6.6 Hz, C_5H_4N), 7.71−7.57 (6 H, m, Ph and CH), 7.36 (1 H, d, J = 16.5 Hz, CH), 7.18 (2 H, d, J = 6.6 Hz, C_5H_4N). ν(C≡N) 2092w, 2058s cm^{-1}. Anal. Calcd (%) for $C_{23}H_{15}N_7FeNa_2\cdot 9H_2O$: C, 42.28; H, 5.09; N, 15.01. Found: C, 41.96; H, 4.44; N, 15.88. TGA analysis indicates the loss of ca. 8.1 molecules of water upon heating.

X-ray Crystallography. Crystals of the salt $Na_2[Fe^{II}(CN)_5(MeQ^+)]\cdot 9H_2O$ (**1**·$9H_2O$) were obtained by diffusion of ethanol vapor into an aqueous solution at 4 °C. A purple block crystal of approximate dimensions 0.60 × 0.60 × 0.10 mm^3 was attached to a Hamilton Cryoloop, using fomblin oil (perfluoropolymethylisopropyl ether) and mounted on a Bruker APEX CCD X-ray diffractometer. Cryocooling to 100 K was carried out by using an Oxford Cryosystems 700 Series cryostream cooler. Intensity measurements were collected by using graphite-monochromated, Mo Kα radiation from a sealed X-ray tube with a monocapillary collimator. The intensities of reflections of a sphere were collected with an exposure time per frame of 5 s. Data processing was carried out by using the Bruker SAINT[14] software package, and a semiempirical absorption correction was applied using SADABS.[14] The structure was solved by direct methods and refined by full-matrix least-squares on all F_0^2 data using SHELXS-97[15] and SHELXL-97.[16] All non-hydrogen atoms were refined anisotropically, with hydrogen atoms bonded to carbon included in calculated positions using the riding method; those bonded to the water oxygen atoms were found by difference Fourier methods and refined isotropically. All other calculations were carried out by using the SHELXTL package.[17] Crystallographic data and refinement details are presented in Table S1.

Hyper-Rayleigh Scattering. Details of the hyper-Rayleigh scattering (HRS) experiment have been discussed elsewhere,[18] and the experimental procedure used was as previously described.[19] β values were determined by using the electric-field-induced second harmonic genera-

(14) *SAINT* (Version 6.45) and *SADABS* (Version 2.10); Bruker AXS, Inc.; Madison, WI, 2003.
(15) Sheldrick, G. M. *Acta Crystallogr., Sect. A* **1990**, *46*, 467−473.
(16) Sheldrick, G. M. *SHELXL 97, Program for crystal structure refinement*; University of Göttingen: Göttingen, Germany, 1997.
(17) *SHELXTL* (Version 6.10); Bruker AXS, Inc.; Madison, WI, 2000.

tion β_{1064} for *p*-nitroaniline (pNA, 32.0×10^{-30} esu in methanol)[20] as an external reference. In the absence of a suitable reference for aqueous solutions, the β_{1064} values in water were obtained by using the β_{1064} for pNA in acetonitrile as an external reference.[20] The absolute magnitudes of these data are hence of questionable accuracy and should be compared only cautiously with the data obtained in methanol. The values for methanol solutions were determined by using the β_{1064} for pNA in methanol.[20] All measurements were performed by using the 1064 nm fundamental of an injection-seeded, *Q*-switched Nd:YAG laser (Quanta-Ray GCR-5, 8 ns pulses, 7 mJ, 10 Hz). Dilute methanol or aqueous solutions (10^{-5}−10^{-6} M) were used to ensure a linear dependence of $I_{2\omega}/I_{\omega}^2$ on solute concentration, precluding the need for Lambert−Beer correction factors. Samples were filtered (Millipore, 0.45 μm), and none showed any fluorescence. One-dimensional hyperpolarizability is assumed, i.e., $\beta_{1064} = \beta_{zzz}$, and a relative error of ±15% is estimated.

For the β switching studies, due to negligible HRS signals from the protonated samples when using a fundamental wavelength of 1064 nm, measurements were instead carried out by using a 800 nm Ti^{3+}:sapphire laser. Samples of **1**−**4** (5 mg) were dissolved in water (20 mL), and portions (8 mL) of these solutions were acidified by the addition of concentrated HCl (2 mL). Reversibility of the switching effect was demonstrated with salt **4** as follows. Four samples (numbered 1−4) of the stock solution (each 3 mL) were placed in 10 mL capacity volumetric flasks. Concentrated HCl (1 drop) was added to three of these samples (2−4), and then samples 3 and 4 were neutralized by the addition of triethylamine until their blue colors were completely restored. Concentrated HCl (1 drop) was then added to sample 4, and all four samples were diluted up to 10 mL so that each contained the same concentration of the complex species.

Stark Spectroscopy. The Stark apparatus, experimental methods, and data analysis procedure were as previously reported,[21,22] with the only modification being that a Xe arc lamp was used as the light source in the place of a W filament bulb. Glycerol−water (50:50 vol %) was used as the glassing medium, for which the local field correction, f_{int}, is estimated as 1.33.[22] The Stark spectrum for each compound was measured a minimum of three times using different field strengths, and the signal was always found to be quadratic in the applied field. A two-state analysis of the MLCT transitions gives

$$\Delta\mu_{ab}{}^2 = \Delta\mu_{12}{}^2 + 4\mu_{12}{}^2 \quad (1)$$

where $\Delta\mu_{ab}$ is the dipole moment difference between the diabatic states corresponding with the effective (localized) electron-transfer process, $\Delta\mu_{12}$ is the observed (adiabatic) dipole moment difference corresponding with a delocalized electron-transfer, and μ_{12} is the transition dipole moment. Analysis of the Stark spectra in terms of the Liptay treatment[23] affords $\Delta\mu_{12}$, and μ_{12} can be determined from the oscillator strength, f_{os}, of the transition by

$$|\mu_{12}| = [f_{os}/(1.08 \times 10^{-5} E_{max})]^{1/2} \quad (2)$$

where E_{max} is the energy of the MLCT maximum (in wavenumbers). The degree of delocalization, $c_b{}^2$, and electronic coupling matrix element, H_{ab}, for the diabatic states are given by

$$c_b{}^2 = \frac{1}{2}\left[1 - \left(\frac{\Delta\mu_{12}{}^2}{\Delta\mu_{12}{}^2 + 4\mu_{12}{}^2}\right)^{1/2}\right] \quad (3)$$

$$|H_{ab}| = \left|\frac{E_{max}(\mu_{12})}{\Delta\mu_{ab}}\right| \quad (4)$$

If the hyperpolarizability tensor, β_0, has only nonzero elements along the MLCT direction, then this quantity is given by

$$\beta_0 = \frac{3\Delta\mu_{12}(\mu_{12})^2}{(E_{max})^2} \quad (5)$$

A relative error of ±20% is estimated for the β_0 values derived from the Stark data and using eq 5, while experimental errors of ±10% are estimated for μ_{12}, $\Delta\mu_{12}$, and $\Delta\mu_{ab}$, ±15% for H_{ab}, and ±50% for $c_b{}^2$.

For the experiments with acidified samples, slides spin-coated with α-cyanoacrylate were used initially because the acid etches the ITO coating off the slides in about 30 min. However, it was subsequently found that rapid freezing of the sample obviates the need for this protective measure. Aliquots (50 μL) of concentrated HCl were added to the blue (500 μL) sample solutions to give orange solutions. Upon further acid addition, precipitates formed, likely the diprotonated neutral complexes $Fe^{II}(CN)_3(CNH)_2L$ (L = MeQ^+, etc.). Some of the samples precipitated immediately after addition of the first aliquot of HCl, precluding measurements, and all samples precipitated out over the course of a few hours. More dilute solutions, such as those originally used to test the effects of acidification via UV−vis spectroscopy or for the HRS experiments, do not show any precipitation.

Computational Procedures. All calculations were performed by using the Gaussian 03[24] program. The molecular geometries were optimized by using the hybrid functional B3P86[25] and the 6-31G* basis set. The B3P86/6-311+G* model chemistry was used for properties calculations. Electronic transitions were calculated by means of the time-dependent density functional theory (TD-DFT) method, and the excited-state dipole moments were calculated either by using the one-particle RhoCI density or the finite-field method which involved the evaluation of the changes in excitation energies in the presence of external electric fields of 0.001 atomic units. The default Gaussian 03 parameters were used in every case. For the calculations on the doubly protonated complex denoted $\mathbf{1}H_2$, protons were placed on the trans cyanide ligand and one of the cis cyanides. The X-ray crystal structure of $\mathbf{1}\cdot 9H_2O$ indicates that there is greater π-back-bonding to the trans cyanide ligand (see below), suggesting that this ligand will be more basic and hence the site of the initial protonation. Molecular orbital contours were plotted by using Molekel 4.3.[26]

Results and Discussion

Synthetic Studies. We have previously reported syntheses of the pro-ligand salts, [2,4-DNPhQ$^+$]Cl and [Phbpe$^+$]Cl,[11,12] but include here modified and improved methods which afford these compounds in yields two to four times higher than those already published. The new complex salts **1**−**6** (Figure 1) were prepared simply by substitution of the ammine ligand in the precursor $Na_3[Fe^{II}(CN)_5(NH_3)]$. The identity and purity of the products are established by diagnostic ^{1}H NMR spectra and CHN elemental analyses. The latter all show the presence of

(18) (a) Clays, K.; Persoons, A. *Phys. Rev. Lett.* **1991**, *66*, 2980−2983. (b) Clays, K.; Persoons, A. *Rev. Sci. Instrum.* **1992**, *63*, 3285−3289. (c) Hendrickx, E.; Clays, K.; Persoons, A.; Dehu, C.; Brédas, J.-L. *J. Am. Chem. Soc.* **1995**, *117*, 3547−3555. (d) Hendrickx, E.; Clays, K.; Persoons, A. *Acc. Chem. Res.* **1998**, *31*, 675−683.
(19) Houbrechts, S.; Clays, K.; Persoons, A.; Pikramenou, Z.; Lehn, J.-M. *Chem. Phys. Lett.* **1996**, *258*, 485−489.
(20) Ståhelin, M.; Burland, D. M.; Rice, J. E. *Chem. Phys. Lett.* **1992**, *191*, 245−250.
(21) Coe, B. J.; Harris, J. A.; Brunschwig, B. S. *J. Phys. Chem. A* **2002**, *106*, 897−905.
(22) Shin, Y.-g. K.; Brunschwig, B. S.; Creutz, C.; Sutin, N. *J. Phys. Chem.* **1996**, *100*, 8157−8169.
(23) (a) Liptay, W. In *Excited States*; Lim, E. C., Ed.; Academic Press: New York, 1974; Vol. 1, pp 129−229. (b) Bublitz, G. U.; Boxer, S. G. *Annu. Rev. Phys. Chem.* **1997**, *48*, 213−242.
(24) Frisch, M. J.; et al. *Gaussian 03*, revision B.05; Gaussian, Inc.: Pittsburgh, PA, 2003.
(25) The B3P86 Functional consists of Becke's three-parameter hybrid functional (Becke, A. D. *J. Chem. Phys.* **1993**, *98*, 5648−5652) with the nonlocal correlation provided by the Perdew 86 expression: Perdew, J. P. *Phys. Rev. B* **1986**, *33*, 8822−8824.
(26) Portmann, S.; Lüthi, H. P. *Chimia* **2000**, *54*, 766−770.

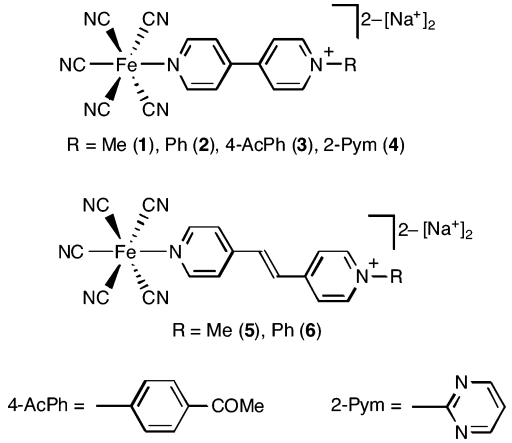

Figure 1. Chemical structures of the Fe^{II} complex salts investigated.

large amounts of water of crystallization, as found in previous investigations with related compounds,[5a,5n,6] and also evidenced by TGA studies.

Electronic Spectroscopy Studies. The UV−vis absorption spectra of complex salts **1**−**6** have been measured in both water and methanol, and the results are shown in Tables 1 and 2. These spectra feature intense UV absorptions due to $\pi \rightarrow \pi^*$ intraligand transitions, together with intense, broad $d(Fe^{II}) \rightarrow \pi^*(L)$ (L = pyridyl ligand) visible MLCT bands.

Within the 4,4′-bipyridinium series **1**−**4**, the MLCT E_{max} values in either solvent decrease as R changes in the order Me > Ph > 4-AcPh > 2-Pym. The magnitude of the total decrease along this series is ca. 0.35 eV in both solvents. This trend reflects the steadily increasing electron deficiency of the pyridinium unit, as observed previously in complexes of these ligands with Ru^{II} ammine[12] or *trans*-$\{Ru^{II}Cl(pdma)_2\}^+$ [pdma = 1,2-phenylenebis(dimethylarsine)][27] electron donor centers. The addition of an (*E*)-CH=CH unit between the two pyridyl rings in moving from **1** to **5** or from **2** to **6** causes insignificant or very small changes in E_{max}, again as observed previously in related compounds.[12,28]

The potential for pronounced interactions between the cyanide ligands and the solvent medium renders **1**−**6** very strongly solvatochromic, with large red-sifts of ca. 0.50 eV in the MLCT bands on moving from water to methanol (Tables 1 and 2). These shifts are also generally accompanied by significant increases in intensity. Decreases in the MLCT E_{max} indicate increasing electron density at the Fe^{II} center, and the difference between the two solvents may be attributed at least in part to the greater H-bond donating ability of water acting to reduce the basicity and enhance the π-accepting ability of the cyanide ligands. Another factor that may be important in this context is the Gutmann electron acceptor number of the solvent.[29] It is known that the MLCT E_{max} (and the $Fe^{III/II}$ potential, see below)

Table 1. UV−Vis Absorption and Electrochemical Data for **1**−**6** in Water

complex salt (L)	λ_{max}, nm (ϵ, M^{-1} cm^{-1})[a]	E_{max} (eV)[a]	assignment	*E*, V vs. Ag/AgCl (ΔE_p, mV)[b] $E_{1/2}[Fe^{III/II}]$	$E_{1/2}$ or E_{pc}[c]
1 (MeQ^+)	534 (3700)	2.32	$d \rightarrow \pi^*$	0.48 (190)	−0.90 (320)
	266 (16 300)	4.66	$\pi \rightarrow \pi^*$		−1.42
2 (PhQ^+)	566 (3900)	2.19	$d \rightarrow \pi^*$	0.48 (140)	−0.86 (250)
	282 (18 700)	4.40	$\pi \rightarrow \pi^*$		−0.74
3 (4-$AcPhQ^+$)	584 (4900)	2.12	$d \rightarrow \pi^*$	0.46 (160)	−0.78
	284 (32 300)	4.37	$\pi \rightarrow \pi^*$		
4 (2-$PymQ^+$)	618 (6400)	2.01	$d \rightarrow \pi^*$	0.46 (130)	−0.61
	290 (32 800)	4.28	$\pi \rightarrow \pi^*$		
5 ($Mebpe^+$)	538 (5000)	2.30	$d \rightarrow \pi^*$	0.45 (130)	−0.94
	318 (26 800)	3.90	$\pi \rightarrow \pi^*$		
	232 (16 300)	5.34	$\pi \rightarrow \pi^*$		
6 ($Phbpe^+$)	562 (6600)	2.21	$d \rightarrow \pi^*$	0.45 (140)	−0.82
	334 (37 600)	3.71	$\pi \rightarrow \pi^*$		
	232 (21 100)	5.34	$\pi \rightarrow \pi^*$		

[a] Solutions ca. $3-8 \times 10^{-5}$ M. [b] Solutions ca. 10^{-3} M in 1 M aqueous KNO_3 at a glassy carbon disk working electrode with a scan rate of 200 mV s^{-1}. [c] For an irreversible reduction process.

Table 2. UV−Vis Absorption and Electrochemical Data for **1**−**6** in Methanol

complex salt (L)	λ_{max}, nm (ϵ, M^{-1} cm^{-1})[a]	E_{max} (eV)[a]	assignment	*E*, V vs Ag/AgCl (ΔE_p, mV)[b] $E_{1/2}[Fe^{III/II}]$	$E_{1/2}$ or E_{pc}[c]
1 (MeQ^+)	686 (5800)	1.81	$d \rightarrow \pi^*$	0.28 (130)	−0.72 (140)
	270 (17 900)	4.59	$\pi \rightarrow \pi^*$		
2 (PhQ^+)	738 (6600)	1.68	$d \rightarrow \pi^*$	0.29 (140)	−0.53 (160)
	290 (21 800)	4.28	$\pi \rightarrow \pi^*$		
3 (4-$AcPhQ^+$)	771 (6300)	1.61	$d \rightarrow \pi^*$	0.31 (110)	−0.43 (150)
	291 (26 000)	4.26	$\pi \rightarrow \pi^*$		
4 (2-$PymQ^+$)	854 (7300)	1.45	$d \rightarrow \pi^*$	0.30 (110)	−0.23 (140)
	293 (24 900)	4.23	$\pi \rightarrow \pi^*$		
5 ($Mebpe^+$)	685 (5800)	1.81	$d \rightarrow \pi^*$	0.24 (150)	−0.60
	319 (27 500)	3.89	$\pi \rightarrow \pi^*$		
	228 (18 700)	5.44	$\pi \rightarrow \pi^*$		
6 ($Phbpe^+$)	742 (6500)	1.67	$d \rightarrow \pi^*$	0.25 (120)	−0.52
	336 (35 400)	3.69	$\pi \rightarrow \pi^*$		
	231 (18 900)	5.37	$\pi \rightarrow \pi^*$		

[a] Solutions ca. $3-8 \times 10^{-5}$ M. [b] Solutions ca. 10^{-3} M in 0.1 M $[NBu^n_4]PF_6$ in methanol at a glassy carbon disk working electrode with a scan rate of 200 mV s^{-1}. Ferrocene internal reference $E_{1/2} = 0.67$ V, $\Delta E_p = 130$ mV. [c] For an irreversible reduction process.

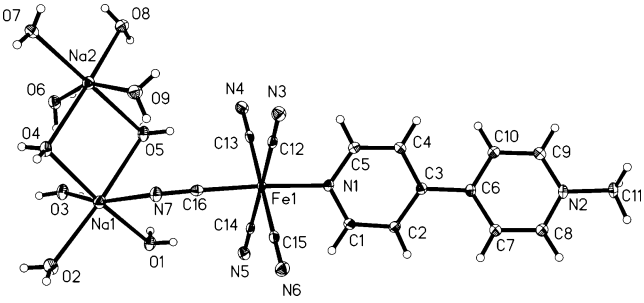

Figure 2. Representation of the molecular structure of **1**·9H_2O (50% probability ellipsoids).

increase with acceptor number for $\{Fe^{II}(CN)_5\}^{3-}$ complexes,[5j,m,n] and water has a higher acceptor number (54.8) than methanol (41.3). As with H-bonding, the better acceptor ability of water will also reduce the electron-donating ability and increase the accepting ability of the cyanide ligands, thus decreasing the electron density at the Fe^{II} center. As expected, the energies of the largely nondirectional intraligand transitions show little solvent sensitivity.

Electrochemical Studies. The complex salts **1**−**6** were studied by cyclic voltammetry in both water and methanol, and the results are presented in Tables 1 and 2. In all cases, reversible or quasireversible $Fe^{III/II}$ waves are observed, the $E_{1/2}$ values of which are almost insensitive to the nature of the pyridyl ligand. However, for each compound, $E_{1/2}[Fe^{III/II}]$ decreases by ca. 200 mV on moving from water to methanol, indicating marked destabilization of the Fe-based HOMOs. This observation can be rationalized by following the same logic regarding solvent−solute interactions as applied to the MLCT energies (see above). Waves assigned to reductions of the pyridinium ligands are also observed and, although these are less well-behaved than the $Fe^{III/II}$ waves, increases of ca. 200 mV on moving from water to methanol are evident. The large accompanying red-shifts in the MLCT bands are therefore attributable to destabilization of the Fe-based HOMOs *and* simultaneous stabilization of the ligand-based LUMOs. Within the 4,4′-bipyridinium series **1**−**4**, the $E_{1/2}$ values for pyridinium ligand-based reduction in methanol increase as R changes in the order Me < Ph < 4-AcPh < 2-Pym. This trend is consistent with the increasing electron-accepting strength of the pyridinium unit, as observed previously in related complexes.[12,27]

Crystallographic Study. A single-crystal X-ray structure has been obtained for the complex salt **1**·9H_2O. A representation of the molecular structure is shown in Figure 2, and selected interatomic distances and angles are presented in Table S2. Although several structures of salts containing $\{Fe^{II}(CN)_5\}^{3-}$ moieties (mostly $[Fe^{II}(CN)_6]^{4-}$ compounds) have been published previously,[5l−n] to our knowledge this is only the second reported structure of a compound containing a $\{Fe^{II}(CN)_5\}^{3-}$ unit coordinated to a pyridyl ligand; the salt $[Et_4N]_3[Fe^{II}(CN)_5(py)]$ (py = pyridine) has been described only very recently.[30]

The Fe−C bond located trans to the MeQ^+ ligand is shorter than the other four Fe−C bonds by ca. 0.03 Å. This phenomenon can be ascribed to the relative structural trans effects of the cyanide and MeQ^+ ligands;[31] the latter is a weaker π-acceptor, and therefore, more extensive π-back-bonding occurs to the trans cyanide when compared with the cis ones. The slightly larger relative trans Fe−C bond shortening of ca. 0.05 Å in $[Et_4N]_3[Fe^{II}(CN)_5(py)]$[30] is consistent with the weaker π-acceptor ability of py when compared with MeQ^+, and the corresponding difference of 0.06 Å in $Na_2[Fe^{II}(CN)_5(NH_3)]\cdot 7H_2O$[5l] is in keeping with the complete absence of π-acceptor character for an ammonia ligand. A smaller and probably insignificant trans Fe−C bond shortening has been observed in $Na_2[Fe^{II}(CN)_5(NO)]\cdot 2H_2O$,[32] consistent with the strong π-accepting ability of a linearly coordinated nitrosyl ligand. As also observed in $[Et_4N]_3[Fe^{II}(CN)_5(py)]$,[30] the plane of the coordinated pyridyl ring in **1**·9H_2O approximately bisects the equatorial C−Fe−C angles.

The MeQ^+ ligand shows no significant evidence for ground-state charge-transfer, with a dihedral angle of 24.26(4)° between the two pyridyl rings. Reported crystal structures for other related complexes such as *trans*-$[Ru^{II}(NH_3)_4(MeQ^+)(PTZ)][PF_6]_3\cdot Me_2CO$[33] (PTZ = *S*-coordinated phenothiazine), *trans*-$[Ru^{II}Cl(pdma)_2(MeQ^+)][PF_6]_2$,[27] and $[Re^{I}(CO)_3(bpy)(MeQ^+)][PF_6]_2$[34] (bpy = 2,2′-bipyridyl) have shown that the dihedral angle within coordinated MeQ^+ can vary over a wide range of ca. 8−44°. One of the sodium countercations is coordinated by six water molecules (two shared with the other sodium cation), and the other cation is coordinated by five water molecules and the N atom of the trans cyanide ligand. A network of hydrogen bonds between these water molecules and the N atoms of the cyanide ligands links the complex units together in a centrosymmetric structure which is unfortunately not expected to display significant bulk NLO effects.

Hyper-Rayleigh Scattering Studies. Complex salts **1**−**6** were studied in both water and methanol by using the HRS technique[18,19] with a 1064 nm Nd:YAG laser fundamental. Values of β_0 were obtained by using the two-state model,[35] and the results are presented in Table 3. Although the applicability of this model has recently been challenged,[36] it remains a viable tool when considering the molecular NLO responses of simple dipolar chromophores which possess a single major ICT band, such as those in **1**−**6**.[37] Furthermore, our previous extensive studies with related Ru^{II} complexes give ample precedent that such an analytical approach is reasonable, and generally affords good results even when working with colored chromophores (as verified by complementary Stark spectroscopic studies).[2m,4,11,12,28,33]

Despite the uncertainties introduced by using β_{1064} for pNA in acetonitrile as an external reference for the data obtained in water, the clearest conclusion to emerge from these HRS data

(27) Coe, B. J.; Beyer, T.; Jeffery, J. C.; Coles, S. J.; Gelbrich, T.; Hursthouse, M. B.; Light, M. E. *J. Chem. Soc., Dalton Trans*. **2000**, 797−803.
(28) Coe, B. J.; Harries, J. L.; Harris, J. A.; Brunschwig, B. S.; Coles, S. J.; Light, M. E.; Hursthouse, M. B. *Dalton Trans*. **2004**, 2935−2942.
(29) (a) Gutmann, V. *Electrochim. Acta* **1976**, *21*, 661−670. (b) Gutmann, V. *The Donor−acceptor Approach to Molecular Interactions*; Plenum: New York, 1978. (c) Gutmann, V.; Resch, G.; Linert, W. *Coord. Chem. Rev.* **1982**, *43*, 133−164.
(30) Chiarella, G. M.; Melgarejo, D. Y.; Koch, S. A. *J. Am. Chem. Soc.* **2006**, *128*, 1416−1417.
(31) Coe, B. J.; Glenwright, S. J. *Coord. Chem. Rev.* **2000**, *203*, 5−80.
(32) Bottomley, F.; White, P. S. *Acta Crystallogr., Sect. B* **1979**, *35*, 2193-2195.
(33) Coe, B. J.; Chamberlain, M. C.; Essex-Lopresti, J. P.; Gaines, S.; Jeffery, J. C.; Houbrechts, S.; Persoons, A. *Inorg. Chem.* **1997**, *36*, 3284−3292.
(34) Busby, M.; Liard, D. J.; Motevalli, M.; Toms, H.; Vlcek, A., Jr. *Inorg. Chim. Acta* **2004**, *357*, 167−176.
(35) (a) Oudar, J. L.; Chemla, D. S. *J. Chem. Phys.* **1977**, *66*, 2664−2668. (b) Oudar, J. L. *J. Chem. Phys*. **1977**, *67*, 446−457.
(36) Selected examples: (a) Meshulam, G.; Berkovic, G.; Kotler, Z. *Opt. Lett.* **2001**, *26*, 30−32. (b) Woodford, J. N.; Wang, C. H.; Jen, A. K.-Y. *Chem. Phys.* **2001**, *271*, 137−143.
(37) Di Bella, S. *New J. Chem.* **2002**, *26*, 495−497.

Table 3. MLCT Absorption and HRS Data for **1**−**6**

	water			methanol		
complex salt (L)	λ_{max} (nm)	β_{1064}[a] (10^{-30} esu)	β_0[b] (10^{-30} esu)	λ_{max} (nm)	β_{1064}[a] (10^{-30} esu)	β_0[b] (10^{-30} esu)
1 (MeQ^+)	534	311	2[c]	686	330	128
2 (PhQ^+)	566	228	22	738	339	163
3 (4-$AcPhQ^+$)	584	218	31	771	728	380
4 (2-$PymQ^+$)	618	214	50	854	485	272
5 ($Mebpe^+$)	538	239	4[c]	685	363	140
6 ($Phbpe^+$)	562	259	22	742	396	192

[a] From 1064 nm HRS measurements at 295 K. [b] Derived from β_{1064} by using the two-state model.[35] [c] Underestimated due to proximity of λ_{max} to 532 nm.

Table 4. MLCT Absorption and Stark Spectroscopic Data for **1**−**6**[a]

complex salt (L)	λ_{max} (nm)	E_{max} (eV)	f_{os}[b]	μ_{12}[c] (D)	$\Delta\mu_{12}$[d] (D)	$\Delta\mu_{ab}$[e] (D)	r_{12}[f] (Å)	r_{ab}[g] (Å)	c_b^2[h]	H_{ab}[i] (cm^{-1})	β_0[j] (10^{-30} esu)
1 (MeQ^+)	533	2.33	0.11	3.5	22.5	23.6	4.7	4.9	0.02	2800	61
2 (PhQ^+)	559	2.22	0.13	4.0	23.5	24.8	4.9	5.2	0.03	2900	88
3 (4-$AcPhQ^+$)	581	2.13	0.14	4.1	26.3	27.5	5.5	5.7	0.03	2600	114
4 (2-$PymQ^+$)	617	2.01	0.17	4.7	26.5	28.1	5.5	5.8	0.03	2700	166
5 ($Mebpe^+$)	557	2.23	0.16	4.4	25.9	27.4	5.4	5.7	0.03	2900	119
6 ($Phbpe^+$)	582	2.13	0.19	4.8	29.3	30.9	6.1	6.4	0.02	2700	174

[a] In glycerol−water (50:50 vol %) glasses at 77 K. Values of E_{max}(eV) for solutions at 295 K: 2.21 (**1**); 2.06 (**2**); 2.01 (**3**); 1.88 (**4**); 2.20 (**5**); 2.07 (**6**). [b] Obtained from $(4.32 \times 10^{-9}$ M $cm^2)A$ where A is the area under the absorption peak. [c] Calculated from eq 2. [d] Calculated from $f_{int}\Delta\mu_{12}$ by using $f_{int} = 1.33$. [e] Calculated from eq 1. [f] Delocalized electron-transfer distance calculated from $\Delta\mu_{12}/e$. [g] Effective (localized) electron-transfer distance calculated from $\Delta\mu_{ab}/e$. [h] Calculated from eq 3. [i] Calculated from eq 4. [j] Calculated from eq 5.

is that the β_0 values of the new complexes are much larger in methanol than in water. This result is consistent with the large red-shifts in the MLCT bands which, according to eq 5, would be expected to lead to increased NLO responses. Also, increasing the electron-accepting ability of the pyridinium group generally causes β_0 to increase within the 4,4′-bipyridinium series **1**−**4**, again as observed previously in related complexes.[12,28] The data in methanol indicate perhaps a small β_0-enhancing effect of extending the conjugated system by adding a (*E*)-CH═CH unit, but the observed differences may not be experimentally significant.

Stark Spectroscopic Studies. We have studied complex salts **1**−**6** by using Stark spectroscopy on the MLCT bands in glycerol−water (50:50 vol %) glasses at 77 K, and the results are shown in Table 4. Representative absorption spectra, Stark spectra, and spectral components for the salts **1** and **4** are shown in Figure S1. The parameter $\Delta\mu_{ab}$ refers to a transition from a localized ground state (i.e., corrected for the effects of metal−ligand bonding), and this quantity becomes particularly significant when making comparisons with related $\{Ru^{II}(NH_3)_5\}^{2+}$ complexes (see below).

The E_{max} values decrease on glassing of the glycerol−water medium at 77 K. A similar effect has been observed previously with Ru^{II} ammine or arsine complex salts on moving from acetonitrile solutions to butyronitrile glasses.[4,21,22,28] Within the 4,4′-bipyridinium series **1**−**4**, f_{os}, μ_{12}, $\Delta\mu_{12}$, and $\Delta\mu_{ab}$ all increase steadily as E_{max} decreases, and the same trends are observed on moving from **5** to **6**. The latter two compounds also have larger values for all of these parameters when compared with their shorter analogues **1** and **2**, respectively. The values of c_b^2 and H_{ab} are almost constant within the series **1**−**6** and indicate only a rather limited degree of delocalization and electronic coupling.

It is reasonable to assume that the lowest energy (i.e., MLCT) electronic transitions dominate the NLO responses of these chromophores, so β_0 values have been derived by using the two-state eq 5. The general trends to emerge from these data mirror those observed previously with Ru^{II} ammine or arsine complex salts,[4a,d,12,21,28] i.e., β_0 within the 4,4′-bipyridinium series **1**−**4** increases as E_{max} decreases, and β_0 also increases on moving from **5** to **6**. *N*-Arylation is therefore an effective aproach to enhancing quadratic NLO responses in the present Fe^{II} cyanide compounds, as in related Ru^{II} ammine or arsine species. Furthermore, comparison of the data for the pairs **1**/**5** and **2**/**6** indicates that extension of the conjugated π-systems leads to ca. 2-fold increases in β_0.

Protic Switching of Optical Properties Probed by Stark Spectroscopy. The presence of lone pairs of electrons on the nitrogen atoms of the *C*-coordinated CN^- ligands means that $\{Fe^{II}(CN)_5\}^{3-}$ complexes can be reversibly protonated.[5a] Given that this chemical transformation greatly changes the basicity of these ligands, the MLCT properties are affected, and this can be expected to alter the NLO properties. Previous reports of protic switching of NLO behavior in purely organic and metal-based chromophores have appeared,[38] but in only one has a well-understood switching of β been experimentally demonstrated.[38c] We have investigated the effects of protonation in complex salts **1**, **3**, and **4** by using Stark spectroscopy, and the results are presented in Table 5. The experimental conditions were established by model studies at room temperature which showed that the observed changes in the MLCT spectra stabilize under the pH conditions used (i.e., the addition of extra concentrated HCl to take the pH below 1.0 gives no further spectral changes). Previous studies suggest that the species being probed under these conditions are diprotonated,[5k] i.e., the neutral complexes $Fe^{II}(CN)_3(CNH)_2L$ (L = MeQ^+, etc.). The acidified solutions appear quite stable and neutralization with triethy-

(38) (a) Lacroix, P. G.; Lepetit, C.; Daran, J. C. *New J. Chem.* **2001**, *25*, 451−457. (b) Hurst, S. K.; et al. *Organometallics* **2001**, *20*, 4664−4675. (c) Asselberghs, I.; Zhao, Y.-X.; Clays, K.; Persoons, A.; Comito, A.; Rubin, Y. *Chem. Phys. Lett.* **2002**, *364*, 279−283. (d) Hurst, S. K.; Humphrey, M. G.; Morrall, J. P.; Cifuentes, M. P.; Samoc, M.; Luther-Davies, B.; Heath, G. A.; Willis, A. C. *J. Organomet. Chem.* **2003**, *670*, 56−65.

Table 5. MLCT Absorption, Stark Spectroscopic and HRS Data for **1**, **3**, and **4** and Their Protonated Forms

complex salt	λ_{max}[a] (nm)	λ_{max}[b] (nm)	E_{max}[b] (eV)	μ_{12}[b,c] (D)	$\Delta\mu_{12}$[b,d] (D)	$\Delta\mu_{ab}$[e] (D)	c_b^2[f]	H_{ab}[g] (cm^{-1})	β_0[h] (10^{-30} esu)	β_{800}[a,i] (10^{-30} esu)	β_0[a,j] (10^{-30} esu)
1	534	533	2.33	3.5	22.5	23.6	0.02	2800	61	87	38
1H_2[k]	410	432	2.87	2.8	24.4	25.0	0.01	2500	26	35	1[l]
3	584	581	2.13	4.1	26.3	27.5	0.03	2600	114	135	71
3H_2[k]	455	457	2.71	3.1	28.6	29.3	0.01	2300	42	92	18
4	618	617	2.01	4.7	26.5	28.1	0.03	2700	166	211	118
4H_2[m]	500	444	2.79	3.2	29.7	30.4	0.01	2400	47	82	28

[a] In water at 295 K. [b] In glycerol−water (50:50 vol %) glasses at 77 K. [c] Calculated from eq 2. [d] Calculated from $f_{int}\Delta\mu_{12}$ by using $f_{int} = 1.33$. [e] Calculated from eq 1. [f] Calculated from eq 3. [g] Calculated from eq 4. [h] Calculated from eq 5. [i] From 800 nm HRS measurements at 295 K. [j] Derived from β_{800} by using the two-state model.[35] [k] 100 μL of concentrated HCl added to 500 μL of sample solution for Stark studies (2.0 M HCl concentration). [l] Underestimated due to proximity of λ_{max} to 400 nm. [m] 200 μL of concentrated HCl added to 500 μL of sample solution for Stark studies (3.4 M HCl concentration).

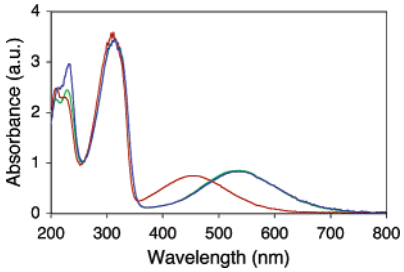

Figure 3. Effects of pH changes on the UV−vis absorption spectrum of **5** in water (ca. 10^{-5} M); original sample at neutral pH (green); acidified to pH < 1.0 by the addition of concentrated HCl (red); basified to pH > 10.0 by the addition of triethylamine (blue).

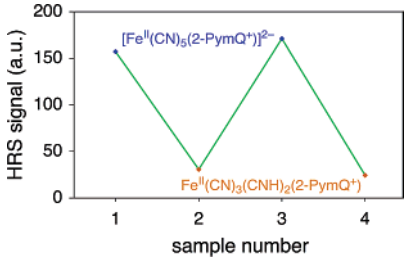

Figure 4. HRS signals derived from the scattering curves shown in Figure S2, with the value for the solvent (water) subtracted.

lamine restores the original spectral profiles which show no additional changes as the pH is increased further (Figure 3).

Protonation causes large increases in E_{max} of ca. 0.5−0.8 eV, consistent with expected decreases in the electron-donating ability of the Fe^{II} center (Figure 3). These blue-shifts are accompanied by decreases in μ_{12} and small increases in $\Delta\mu_{12}$ and $\Delta\mu_{ab}$. The values of c_b^2 and H_{ab} show slight decreases which are in keeping with the expectation that the less electron-rich $\{Fe^{II}(CN)_3(CNH)_2\}^-$ moiety will engage in less effective π-back-bonding when compared with $\{Fe^{II}(CN)_5\}^{3-}$; although the differences for these quantities are within the experimental errors, the consistency of the trends suggests that these may be real. Most importantly, β_0 is found to decrease upon protonation by a factor of ca. 2−4, corresponding with a relatively efficient switching process. This phenomenon is attributable to the increases in E_{max} and decreases in band intensity (i.e., μ_{12}) which are partially offset by the small increases in $\Delta\mu_{12}$.

Protic Switching of First Hyperpolarizabilities Probed by Hyper-Rayleigh Scattering. We have also carried out HRS studies to directly confirm the effects of protonation on the β responses of **1**−**4**, using a 800 nm Ti^{3+}:sapphire laser due to negligible HRS signals from the protonated samples when using a 1064 nm fundamental. The β_0 values for the neutral and acidified solutions were estimated from the β_{800} data by using the two-state model,[35] and the results are presented in Table 5. The data for **2** and **2**H_2 are $\beta_{800}(\beta_0) = 123(62)$ and 66(15) $\times$ 10^{-30} esu, respectively. Reversibility of the switching effect was demonstrated with salt **4**; the quadratic curves for samples 1−4 are shown in Figure S2, and the quadratic coefficients derived from these curves (with the value for the solvent subtracted) are shown in Figure 4.

As noted above, the acidified samples show large increases in E_{max}, and these blue-shifts of the MLCT bands are accompanied by large decreases in β_{800} and (especially) β_0. With the exception of **1**, for which the β_0 of the protonated form (**1**H_2) is grossly underestimated, all of the complexes show ca. 4-fold decreases in their NLO responses upon protonation. The magnitude of these changes is similar to that predicted by the Stark measurements, although the actual β_0 values derived from the latter studies are always higher than those determined via HRS in aqueous solutions.

Theoretical Studies. In previous studies on the NLO properties of dipolar Ru^{II} ammine complexes,[4c,d] we have demonstrated the usefulness of density functional theory (DFT) methods along with the effective core potential (ECP) LanL2DZ. However, this model chemistry is inadequate for studying anionic species which require the use of diffuse functions to reliably predict their NLO behavior. Initial calculations were hence carried out by using the B3P86/6-311+G* model chemistry with geometries that were optimized in the gas phase by using the same functional and the 6-31G* basis set. The hyperpolarizabilities calculated in this way by using the finite-field (FF) approach, $\beta_0 = 104 \times 10^{-30}$ esu for the complex anion in **1** and $\beta_0 = 160 \times 10^{-30}$ esu for that in **5**, are in reasonable agreement with the experimental values derived via HRS in methanol. We have also calculated the electronic transitions for the complex anions in these salts by using TD-DFT and the same level of theory. The estimation of $\Delta\mu_{12}$ values by using either the one-electron RhoCI density or the FF method allows the calculation of β_0 via eq 5. Once again, the results (Table S3) agree reasonably well with the experimental data obtained via HRS in methanol or via Stark spectroscopy. However, this agreement is purely coincidental because the calculated $\Delta\mu_{12}$ values are an order of magnitude smaller than those obtained from Stark studies, while the predicted values of f_{os} and μ_{12} are several times larger than the corresponding experimental data.

In the search for a model that provides better agreement between theory and experiment, we have included solvent effects using a polarizable continuum model (PCM). Initial single-point PCM calculations performed on the geometries optimized in the gas phase provide somewhat larger $\Delta\mu_{12}$ values, but only small changes are observed in the calculated μ_{12} values. For

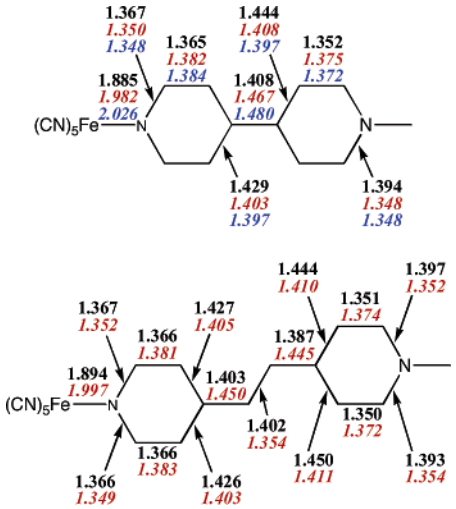

Figure 5. Selected bond lengths in the complex anions in **1** (top) and **5** (bottom), optimized in a vacuum (black) and water (red italics). The crystallographic values for **1** are also shown (blue italics).

example, for the complex anion in **1**, $\Delta\mu_{12}$ increases from 1.2 to 16.7 (calculated by using the RhoCI density), while μ_{12} decreases from 10.2 to 9.7 (Table S3). Better agreement is obtained when calculations are performed on geometries that are optimized by using the PCM method (Table S3). The calculated $\Delta\mu_{12}$ values are now comparable to those determined by the Stark technique, and the values of μ_{12} and f_{os}, while still larger than the experimental ones, are somewhat smaller than those calculated on the gas-phase geometries. However, it must be noted that PCM calculations cannot simulate the effects of H-bonding and the results of these calculations are best compared to the measurements in methanol which, as described above, show E_{max} values that are very close to those calculated and absorptions which are generally more intense than those in water.

Given that molecular geometry has important effects on NLO behavior, it is worth making a detailed comparison of the geometries obtained in the gas phase and in solution. Figure 5 shows selected bond lengths in the optimized geometries of the complex anions in **1** and **5** in the gas phase and in aqueous solutions. It can be seen that passing from gas phase to the polar solvent medium causes dramatic changes in the geometry and that there is a close agreement between the bond lengths calculated in water and those observed in the X-ray crystal structure of **1**·9H_2O (Figure 5 and see above).

Changes in geometry can be rationalized by considering the existence of two limiting resonance structures corresponding to the fully aromatic or quinoidal species (Figure 6). Comparison of the bond lengths shown in Figure 5 indicates that bonds depicted as double in the quinoidal structure are shorter in the

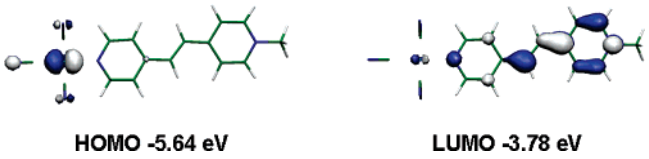

Figure 7. Illustrations of the 0.04 contour plots of molecular orbitals of the complex anion in **5** calculated by PCM(H_2O)-B3P86/6-311+G*.

gas phase than in solution, while those depicted as single are longer in the gas phase. Therefore, polar media, such as water, favor the more polar (charge-separated) structures, while non-polar solvents favor the less-polar structures. In the present complexes, as also observed in some purely organic chromophores,[39] the more-polar structures are aromatic while the less-polar forms are quinoidal.

Further support for the preference of the quinoidal or aromatic structure in different media can be obtained from the calculated charges[40] and also the spatial arrangement of the methyl group (Figure S3). In the aromatic structure, the pyridyl nitrogen attached to this methyl group has sp^2 hybridization and is therefore planar, whereas the nitrogen in the quinoidal structure must have sp^3 hybridization and show a tetrahedral arrangement. As expected, the methyl group lies coplanar with the adjacent pyridyl ring in the solution geometries but moves out of this ring plane by ca. 21° in the gas-phase geometries.

As expected, TD-DFT shows that most of the hyperpolarizability of these molecules is associated with their lowest-energy absorptions which arise from one electron HOMO → LUMO transitions. The topologies of the orbitals involved in these transitions (Figures 7 and 8) show that the HOMOs are mainly derived from iron d orbitals while the LUMOs spread over the MeQ^+/$Mebpe^+$ ligand, confirming the assignment of these transitions as being MLCT character. Although the HOMO−LUMO gap in the complex anion in **1** is larger by 0.29 eV when compared with that in **5**, the increased correlation in the more extended complex anion in **5** reduces the difference in E_{max} calculated by TD-DFT to only ca. 0.1 eV (Table S3), which is in better agreement with the nearly identical E_{max} values observed experimentally for **1** and **5**. The greater length of the complex anion in **5** when compared to that in **1** is responsible for the larger $\Delta\mu_{12}$ and μ_{12} values that give rise to a larger β_0.

To study the protic switching of β in the complex anion in **1**, we have also performed calculations on the monoprotonated, diprotonated, and fully protonated complex species (denoted **1**H, **1**H_2, and **1**H_5, respectively) with the same model chemistry used for the anionic species (PCM-B3P86/6-311+G* on PCM-B3P86/6-31G* geometries). The results of these calculations are summarized in Table 6. TD-DFT reveals that the lowest energy absorption corresponds in every case to a MLCT transition, with the orbitals being those shown in Figure 8. A

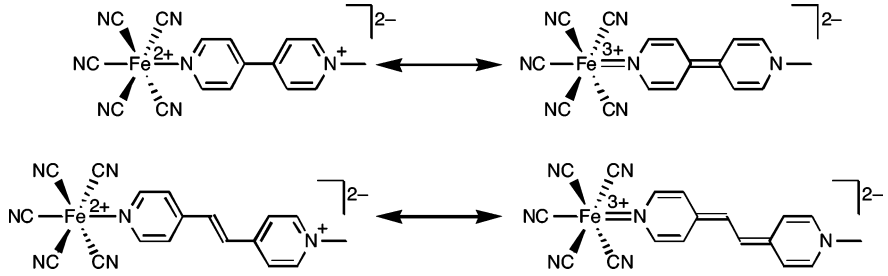

Figure 6. Limiting resonance structures of the complex anions in **1** (top) and **5** (bottom).

Table 6. Results of Theoretical Calculations on the Complex Anion in **1** and Its Protonated Forms

parent salt	HOMO–LUMO gap	E_{max} (eV)	μ_{12} (D)	f_{os}	$\Delta\mu_{12}{}^a$ (D)	$\Delta\mu_{12}{}^b$ (D)	$\beta_0{}^c$ (10^{-30} esu)	$\beta_0{}^d$ (10^{-30} esu)
1	2.15	1.82	6.7	0.31	24.7	17.0	391	269
1H	2.74[e]	2.28	4.0	0.14	28.8	26.3	104	95
1H_2	3.27[e]	2.77	2.4	0.06	29.2	27.4	26	25
	3.46[f]	2.95	2.9	0.09	29.1	27.2	32	30
1H_5	4.65	4.09	4.5	0.32	22.3	26.7	32	38

[a] Calculated by using the RhoCI density. [b] Calculated by using the FF approach. [c] Calculated from eq 5 by using the RhoCI $\Delta\mu_{12}$ value. [d] Calculated from eq 5 by using the FF $\Delta\mu_{12}$ value. [e] (HOMO-1) → LUMO. [f] (HOMO-2) → LUMO.

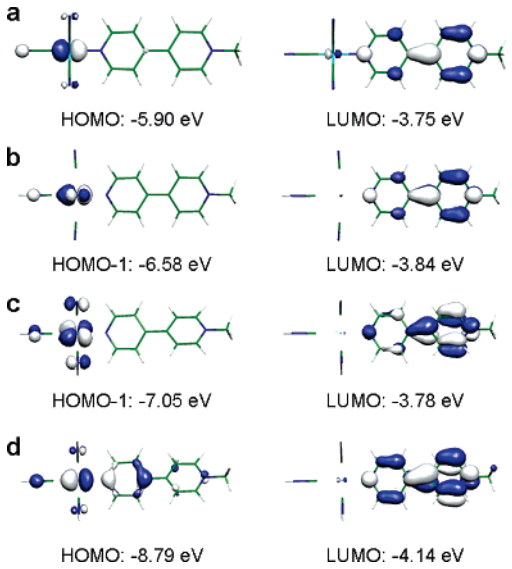

Figure 8. Illustrations of the 0.04 contour plots of molecular orbitals involved in the lowest energy transition of the complex chromophores in **1** (a), **1**H (b), **1**H_2 (c), and **1**H_5 (d) calculated by PCM(H_2O)-B3P86/6-311+G*.

comparison of these orbitals shows that protonation lowers the energies of the Fe^{II}-based orbitals which are located near the protonation site, but the energy of the LUMO located on the MeQ^+ ligand is less affected by the acidity of the medium. As a consequence of these energy changes, the HOMO−LUMO gap increases steadily on protonation from 2.15 to 4.65 eV (in **1**H_5) while the corresponding E_{max} value calculated by TD-DFT changes from 1.82 to 4.09 eV. The calculated blue-shift of 1.05 eV passing from **1** to **1**H_2 is rather larger than the 0.54 eV shift observed at 77 K in glycerol−water (50:50 vol %) (Table 5). Furthermore, the β_0 of 26×10^{-30} esu calculated from eq 5 for **1**H_2 by using the parameters obtained from TD-DFT is strongly decreased with respect to the 391×10^{-30} esu calculated for the anion in **1** via the same methodology, and this dramatic drop in the hyperpolarizability mainly arises from the large blue-shift caused by protonation.

It should be noted, however, that for the neutral species **1**H_2 the predicted excitation energy for the second lowest energy transition is 2.95 eV, which is only 0.18 eV above that of the lowest energy transition, and therefore, the second excited state is expected to have an important contribution to the overall hyperpolarizability. According to our calculations, this second lowest energy transition is mainly comprised of a HOMO-2 to LUMO excitation that also has MLCT character. The calculated $\Delta\mu_{12}$ for this second excitation is similar to that of the (HOMO-1) → LUMO transition described above, but its larger μ_{12} produces a contribution to the hyperpolarizability that is comparable to that of the first allowed transition despite the lower energy of the latter (Table 6). If these two lowest energy MLCT transitions are taken into account, then the total β_0 response predicted for **1**H_2 by using the RhoCI $\Delta\mu_{12}$ values in eq 5 is 58×10^{-30}.

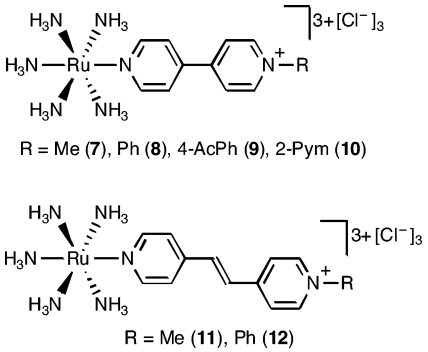

Figure 9. Chemical structures of the Ru^{II} complex salts investigated.

Ruthenium Pentaammine Complexes: Electronic Spectroscopy and Electrochemical Studies. Given that we have previously carried out extensive studies with Ru^{II} ammine complexes of the same pyridinium ligands used here,[4a,d,12,21,28] it is of interest to draw comparisons between these two classes of compounds. However, to do so further, new data have been obtained for the Ru^{II} ammine complex salts under the same experimental conditions as those used to study the Fe^{II} cyanide compounds. To improve the solubility in water and alcohols, we used the chloride salts rather than the previously studied hexafluorophosphates,[41] and UV−vis and electrochemical data for the complex salts **7**−**12** (Figure 9) are presented in Table 7.

(39) Andreu, R.; Blesa, M. J.; Carrasquer, L.; Garín, J.; Orduna, J.; Villacampa, B.; Alcalá, R.; Casado, J.; Ruiz Delgado, M. C.; López Navarrete, J. T.; Allain, M. *J. Am. Chem. Soc.* **2005**, *127*, 8835−8845.

(40) The Mulliken charges (e^-) calculated for the {$Fe(CN)_5$} group by using B3P86/6-311+G* are as follows. Anion in **1**, gas phase −1.844; PCM-(water) −2.859. Anion in **5**, gas phase −1.826; PCM(water) −2.935. These results are consistent with the iron atom having a formal oxidation state of +3 in the gas phase and +2 in water.

(41) It should be noted that some uncertainty exists regarding the precise formulations of the materials $[Ru^{II}(NH_3)_5L]Cl_3$ due to their hygroscopic nature coupled with the well-established difficulties in obtaining satisfactory CHN elemental analyses for such Ru^{II} ammine salts. Previous studies with **7**−**9** indicated that these compounds retain ca. 2.5−3.5 molecules of water of crystallization after drying under vacuum at room temperature.[3a] However, we have repeatedly been unable to obtain satisfactory CHN analyses for **10**−**12**; the consistently low C and N percentages are driven up by as much as 70% of their initial values following prolonged heating under vacuum, with approximately constant C/N ratios, but the expected values are never achieved. Representative data for **11** are as follows. Anal. Calcd (%) for $C_{13}H_{28}Cl_3N_7Ru$: C, 31.88; H, 5.76; N, 20.02. Found after vacuum-drying at room temperature for 24 h: C, 18.87; H, 6.30; N, 10.74. Found after vacuum-drying at 100 °C for 24 h: C, 27.23; H, 4.93; N, 15.50. Given that **7**−**12** are prepared simply by anion metathesis from their PF_6^- counterparts (which are confirmed to be pure by ^{1}H NMR spectra and CHN analyses), there is no reason to doubt the chromophoric purity of **7**−**12**. However, for the purposes of calculating the solution concentrations for physical studies, we make the assumption that all of these samples contain 3 molar equivalents of water of crystallization.

Table 7. UV−Vis Absorption and Electrochemical Data for **7**−**12**

complex salt (L)	λ_{max}, nm (ϵ, M^{-1} cm^{-1})[a]	E_{max} (eV)[a]	λ_{max}, nm (ϵ, M^{-1} cm^{-1})[b]	E_{max} (eV)[b]	assignment	E, V vs. Ag/AgCl (ΔE_p, mV)[c] $E_{1/2}[Ru^{III/II}]$	$E_{1/2}$ or E_{pc}[d]
7 (MeQ^+)	606 (9300)	2.05	622 (9900)	1.99	d → π^*	0.26 (130)	−0.88 (210)
	262 (22 300)	4.73	265 (15 450)	4.68	$\pi \rightarrow \pi^*$		−1.33
8 (PhQ^+)	622 (11 900)	1.99	655 (13 200)	1.89	d → π^*	0.27 (120)	−0.76 (160)
	283 (14 500)	4.38	287 (14 100)	4.32	$\pi \rightarrow \pi^*$		
9 (4-$AcPhQ^+$)	638 (13 200)	1.94	672 (13 300)	1.85	d → π^*	0.29 (110)	−0.71
	287 (18 300)	4.32	291 (14 250)	4.26	$\pi \rightarrow \pi^*$		
10 (2-$PymQ^+$)	677 (13 400)	1.83	715 (13 600)	1.73	d → π^*	0.28 (120)	−0.62
	287 (18 200)	4.32	286 (14 550)	4.34	$\pi \rightarrow \pi^*$		
11 ($Mebpe^+$)	592 (7700)	2.09	625 (10 750)	1.98	d → π^*	0.21 (100)	−0.95
	316 (19 800)	3.92	318 (16 550)	3.90	$\pi \rightarrow \pi^*$		
	227 (9500)	5.46	228 (7250)	5.44	$\pi \rightarrow \pi^*$		
12 ($Phbpe^+$)	620 (13 600)	2.00	657 (14 000)	1.89	d → π^*	0.22 (110)	−0.78
	334 (27 300)	3.71	337 (22 850)	3.67	$\pi \rightarrow \pi^*$		
	230 (9800)	5.39	231 (8600)	5.37	$\pi \rightarrow \pi^*$		

[a] In water ca. $3-8 \times 10^{-5}$ M. [b] In methanol ca. $3-8 \times 10^{-5}$ M. All concentrations calculated by assuming that each sample contains 3 molar equivalents of water of crystallization.[41] Values of E_{max}(eV) for acetonitrile solutions of PF_6^- salts at 295 K: 2.10 (**7**); 1.97 (**8**); 1.90 (**9**); 1.84 (**10**); 2.08 (**11**); 1.97 (**12**).[11,12] [c] Solutions ca. 10^{-3} M in 1 M aqueous KNO_3 at a glassy carbon disk working electrode with a scan rate of 200 mV s^{-1}. Electrochemical data could not be obtained in methanol due to insufficient solubility of these compounds in the electrolyte solution. [d] For an irreversible reduction process.

Table 8. MLCT Absorption and HRS Data for **7**−**12**

	water			methanol		
complex salt (L)	λ_{max} (nm)	β_{1064}[a] (10^{-30} esu)	β_0[b] (10^{-30} esu)	λ_{max} (nm)	β_{1064}[a] (10^{-30} esu)	β_0[b] (10^{-30} esu)
7 (MeQ^+)	606	169	34	622	455	110
8 (PhQ^+)	622	255	62	655	493	158
9 (4-$AcPhQ^+$)	638	333	93	672	522	187
10 (2-$PymQ^+$)	677	402	148	715	497	220
11 ($Mebpe^+$)	592	150	25	625	589	147
12 ($Phbpe^+$)	620	212	50	657	522	170

[a] From 1064 nm HRS measurements at 295 K. [b] Derived from β_{1064} by using the two-state model.[35]

Table 9. MLCT Absorption and Stark Spectroscopic Data for **7**−**12**[a]

complex salt (L)	λ_{max} (nm)	E_{max} (eV)	f_{os}[b]	μ_{12}[c] (D)	$\Delta\mu_{12}$[d] (D)	$\Delta\mu_{ab}$[e] (D)	r_{12}[f] (Å)	r_{ab}[g] (Å)	c_b^2[h]	H_{ab}[i] (cm^{-1})	β_0[j] (10^{-30} esu)
7 (MeQ^+)	633	1.96	0.14	4.3	13.2	15.8	2.8	3.3	0.08	4300	74
8 (PhQ^+)	678	1.83	0.17	4.9	15.2	18.1	3.2	3.8	0.08	4000	129
9 (4-$AcPhQ^+$)	705	1.76	0.35	7.2	14.1	20.1	2.9	4.2	0.15	5000	275
10 (2-$PymQ^+$)	751	1.65	0.25	6.4	15.3	19.9	3.2	4.2	0.12	4300	267
11 ($Mebpe^+$)	653	1.90	0.10	3.8	16.9	18.6	3.5	3.9	0.04	3200	80
12 ($Phbpe^+$)	690	1.80	0.29	6.6	18.2	22.4	3.8	4.7	0.09	4200	282

[a] Measured in glycerol−water (50:50 vol %) glasses at 77 K. All concentrations calculated by assuming that each sample contains 3 molar equivalents of water of crystallization.[41] [b] Obtained from $(4.32 \times 10^{-9}$ M $cm^2)A$ where A is the area under the absorption peak. [c] Calculated from eq 2. [d] Calculated from $f_{int}\Delta\mu_{12}$ by using $f_{int} = 1.33$. [e] Calculated from eq 1. [f] Calculated from $\Delta\mu_{12}/e$. [g] Calculated from $\Delta\mu_{ab}/e$. [h] Calculated from eq 3. [i] Calculated from eq 4. [j] Calculated from eq 5.

The new MLCT absorption data for **7**−**12** show the same trends as observed previously in acetonitrile (i.e., red-shifting with increasing acceptor strength of L),[12] and the E_{max} values in this solvent are similar to those in water but larger by ca. 0.1 eV when compared with those in methanol. The electrochemical data also resemble those obtained in acetonitrile:[12] the $Ru^{III/II}$ $E_{1/2}$ values are smaller for **11** and **12** than for **7**−**10** due to the mildly electron-donating influence of the (*E*)-CH═CH unit, and the ligand reduction potentials decrease as the pyridinium group becomes more electron deficient.

Ruthenium Pentaammine Complexes: Hyper-Rayleigh Scattering Studies. The results of HRS studies at 1064 nm with complex salts **7**−**12** in both water and methanol are presented in Table 8. As with the MLCT absorption data, these new HRS data for **7**−**12** show the same trends as observed previously in acetonitrile (i.e., increasing β_0 with red-shifting of the MLCT band).[12] As expected, the red-shifts in the MLCT bands on moving from water to methanol are accompanied by large increases in β_0, but the actual size of this effect is obscured by the uncertain referencing of the data in water. Interestingly, the effect of inserting a (*E*)-CH═CH unit into the conjugated bridge appears to be different in the two solvents, i.e., decreases in β_0 in water but increases in methanol, although the changes are not large.

Ruthenium Pentaammine Complexes: Stark Spectroscopic Studies. We have also carried out Stark studies with complex salts **7**−**12** in glycerol−water (50:50 vol %) glasses at 77 K, and the results are presented in Table 9. These data show the same general trends as observed when using butyronitrile glasses,[21] although it is worth noting that these are the first Stark results for the complex in **10** because a satisfactory data fit could not be obtained with $[Ru^{II}(NH_3)_5(2\text{-}PymQ^+)][PF_6]_3$.[21] In particular, the now well-established correlation between β_0 and L acceptor strength is again apparent.

Comparisons between Iron Pentacyanide and Ruthenium Pentaammine Complexes. Although these two types of chro-

Table 10. Selected MLCT Absorption, Electrochemical, Stark Spectroscopic, and HRS Data for Complex Salts $Na_2[Fe^{II}(CN)_5L]$ and $[Ru^{II}(NH_3)_5L]Cl_3$

complex salt (L)	E_{max}[w][a] (eV)	E_{max}[m][a] (eV)	E_{max}[g–w][b] (eV)	$E_{1/2}$[$M^{III/II}$][c] (V)	μ_{12}[d] (D)	$\Delta\mu_{12}$[e] (D)	$\Delta\mu_{ab}$[f] (D)	r_{12}[g] (Å)	r_{ab}[h] (Å)	c_b^2[i]	H_{ab}[j] (cm^{-1})	β_0[k] (10^{-30} esu)	β_0[l] (10^{-30} esu)	β_0[m] (10^{-30} esu)
1 (MeQ^+)	2.32	1.81	2.33	0.48	3.5	22.5	23.6	4.7	4.9	0.02	2800	61	2^n	128
7 (MeQ^+)	2.05	1.99	1.96	0.26	4.3	13.2	15.8	2.8	3.3	0.08	4300	74	34	110
2 (PhQ^+)	2.19	1.68	2.22	0.48	4.0	23.5	24.8	4.9	5.2	0.03	2900	88	22	163
8 (PhQ^+)	1.99	1.89	1.83	0.27	4.9	15.2	18.1	3.2	3.8	0.08	4000	129	62	158
3 (4-$AcPhQ^+$)	2.12	1.61	2.13	0.46	4.1	26.3	27.5	5.5	5.7	0.03	2600	114	31	380
9 (4-$AcPhQ^+$)	1.94	1.85	1.76	0.29	7.2	14.1	20.1	2.9	4.2	0.15	5000	275	93	187
4 (2-$PymQ^+$)	2.01	1.45	2.01	0.46	4.7	26.5	28.1	5.5	5.8	0.03	2700	166	50	272
10 (2-$PymQ^+$)	1.83	1.73	1.65	0.28	6.4	15.3	19.9	3.2	4.2	0.12	4300	267	148	220
5 ($Mebpe^+$)	2.30	1.81	2.23	0.45	4.4	25.9	27.4	5.4	5.7	0.03	2900	119	4^n	140
11 ($Mebpe^+$)	2.09	1.98	1.90	0.21	3.8	16.9	18.6	3.5	3.9	0.04	3200	80	25	147
6 ($Phbpe^+$)	2.21	1.67	2.13	0.45	4.8	29.3	30.9	6.1	6.4	0.02	2700	174	22	192
12 ($Phbpe^+$)	2.00	1.89	1.80	0.22	6.6	18.2	22.4	3.8	4.7	0.09	4200	282	50	170

[a] At 295 K; w = water, m = methanol. [b] At 77 K; g–w = glycerol–water (50:50 vol %). [c] Reported vs Ag/AgCl reference; solutions ca. 10^{-3} M in 1 M aqueous KNO_3 at a Pt disk working electrode with a scan rate of 200 mV s^{-1}; M = Fe or Ru. [d] Calculated from eq 2. [e] Calculated from $f_{int}\Delta\mu_{12}$ by using $f_{int} = 1.33$. [f] Calculated from eq 1. [g] Calculated from $\Delta\mu_{12}/e$. [h] Calculated from $\Delta\mu_{ab}/e$. [i] Calculated from eq 3. [j] Calculated from eq 4. [k] Calculated from eq 5. [l] From 1064 nm HRS measurements in water. [m] From 1064 nm HRS measurements in methanol. [n] Underestimated due to proximity of λ_{max} to 532 nm.

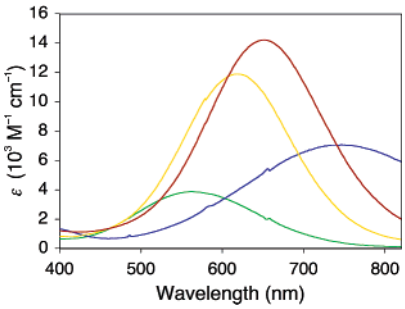

Figure 10. MLCT absorption spectra of complex salts **2** in water (green) and methanol (blue) and **8** in water (gold) and methanol (red).

mophore both contain strongly electron-donating d^6 metal centers, they are clearly quite different chemically, and this might be expected to be reflected in their electronic and optical properties. Several previous comparative studies involving $\{Fe^{II}(CN)_5\}^{3-}$ and $\{Ru^{II}(NH_3)_5\}^{2+}$ complexes have appeared,[5a,d–f,h] but none feature either Stark or HRS results. The general conclusions to emerge from these earlier studies can be summarized as follows. (i) The MLCT bands of the Ru^{II} complexes appear at lower energies than those of their Fe^{II} counterparts (at least in aqueous solutions), and (ii) a $\{Ru^{II}(NH_3)_5\}^{2+}$ center engages in more effective π-back-bonding with pyridyl ligands (i.e., better metal–ligand orbital overlap) when compared with $\{Fe^{II}(CN)_5\}^{3-}$ due primarily to the larger radial extension of 4d as opposed to 3d orbitals. The back-bonding ability of the Fe^{II} center may also be reduced by the fact that the cyanide co-ligands also possess π-acceptor properties. The physical studies that we now report allow unprecedentedly detailed comparisons to be made, and selected data are collected in Table 10 for this purpose. Representative UV–vis spectra of complex salts **2** and **8** in water and methanol are shown in Figure 10.

All of the MLCT absorption data obtained in aqueous solutions at 295 K or in glycerol–water (50:50 vol %) glasses at 77 K are in agreement with previous reports in that the Ru^{II} compounds always have considerably lower E_{max} values when compared with their Fe^{II} counterparts. The $\{Ru^{II}(NH_3)_5\}^{2+}$ vs $\{Fe^{II}(CN)_5\}^{3-}$ energy differences are ca. 0.2–0.3 and 0.3–0.4 eV in water and glycerol–water, respectively. However, this situation is completely reversed in methanol because the red-shifting of the MLCT bands is much more pronounced for the Fe^{II} compounds, meaning that the E_{max} values for the Ru^{II} complexes are now higher than those of their Fe^{II} counterparts by ca. 0.2–0.3 eV (Figure 10). Hence, if only MLCT energies are considered, then a $\{Ru^{II}(NH_3)_5\}^{2+}$ center is a stronger electron donor than a $\{Fe^{II}(CN)_5\}^{3-}$ moiety in water or glycerol–water, but the opposite is true in methanol. The observation that the $E_{1/2}$ potentials for metal-based oxidation in aqueous solution are lower by ca. 0.2 V for the Ru complexes than for their Fe congeners is also consistent with the greater electron-richness (and by inference electron-donating ability) of the $\{Ru^{II}(NH_3)_5\}^{2+}$ center under such conditions.

With the exception of **11**, the derived values of μ_{12}, c_b^2, and H_{ab} are larger in the Ru^{II} complexes than in their Fe^{II} counterparts; these observations are consistent with previous studies which conclude that π-orbital overlap is more effective with the $\{Ru^{II}(NH_3)_5\}^{2+}$ center. $\Delta\mu_{12}$ relates to a transition from a delocalized ground state, and $\Delta\mu_{ab}$ refers to a transition from a localized ground state (i.e., corrected for the effects of metal–ligand bonding). These two quantities are interrelated by c_b^2, the degree of delocalization by eq 6.

$$\Delta\mu_{ab} = \frac{\Delta\mu_{12}}{1 - 2c_b^2} \qquad (6)$$

In every case, the values of $\Delta\mu_{12}$ and $\Delta\mu_{ab}$ decrease quite considerably on moving from a $\{Fe^{II}(CN)_5\}^{3-}$ complex to its $\{Ru^{II}(NH_3)_5\}^{2+}$ analogue, and hence, the electron-transfer distances, r_{12} and r_{ab}, are also smaller for the Ru^{II} complexes. The r values indicate that in the Ru^{II} complexes the charge is transferred onto the first pyridyl ring, whereas in their Fe^{II} counterparts, the charge is transferred further toward the middle of L. The decrease in $\Delta\mu_{12}$ is potentially a consequence of increased delocalization due to stronger π-back-bonding in the Ru^{II} complexes. The amount of charge transferred is given by $(1 - 2c_b^2)e$, so as the degree of delocalization, c_b^2, increases, less charge is transferred and $\Delta\mu_{12}$ decreases. The difference between $\Delta\mu_{12}$ and $\Delta\mu_{ab}$ also increases on replacing $\{Ru^{II}(NH_3)_5\}^{2+}$ with $\{Fe^{II}(CN)_5\}^{3-}$. The use of $\Delta\mu_{ab}$ allows 'correction' of the dipole moment change for the manner of bonding and the extent of delocalization between the metal and L.[22] Therefore, if the only difference between the Fe^{II} and Ru^{II} complexes were the increased π-back-bonding interaction of the Ru^{II} center, then the two types of complexes should display

similar $\Delta\mu_{ab}$ values. The fact that this is not the case indicates that another effect must also be contributing to the decreased $\Delta\mu_{12}$ values observed for the Ru^{II} species.

The other effect which influences $\Delta\mu_{12}$ is likely to be repolarization of the L valence electrons in the excited state. Because an MLCT state formally contains a M^{III} center, the valence electrons on L will be displaced as a consequence of the increased positive charge at the metal. This repolarization of the ligand valence electrons causes its electron distribution to shift toward the metal, resulting in a dipole moment change which opposes that produced by the MLCT excitation process, thus decreasing the observed $\Delta\mu_{12}$.[42] In the case of the Fe complexes, the π electrons within the CN^- ligands are more easily polarized (when compared to NH_3 which lacks π electrons) and therefore stabilize the increased charge on the Fe^{III} center in the excited state. Thus, L experiences a smaller increase in positive charge in the excited state when compared with the Ru^{III} case and is not polarized to the same extent as in the Ru complexes.

Except for **11**, the β_0 values derived from the Stark data by using eq 5 are larger (and in most cases substantially so) for the Ru^{II} complexes than for their Fe^{II} counterparts. This trend arises because the β_0-enhancing effects of decreased E_{max} and increased μ_{12} values more than offset the decreases of $\Delta\mu_{12}$ in the Ru^{II} complexes. The HRS experiments in water concur with this general result, i.e., $\{Ru^{II}(NH_3)_5\}^{2+}$ is a more effective electron donor than $\{Fe^{II}(CN)_5\}^{3-}$ in terms of quadratic NLO responses. However, the HRS data in methanol present an opposite picture (with the exception of **5**) in that the Fe^{II} center becomes the better electron donor, although in most cases, the differences are not very large. This change in relative behavior of β_0 obviously correlates with the solvatochromic properties of the compounds under study; the very large red-shifts in the MLCT bands of the Fe^{II} complexes on moving from water to methanol mean that their $\{Ru^{II}(NH_3)_5\}^{2+}$ analogues become the higher-energy absorbers. Although it would clearly be of interest to also determine $\Delta\mu_{12}$ values for **1**−**12** in water and methanol, this is unfortunately precluded by the requirement of Stark spectroscopy for suitable glassing media.

It is also worth noting that it is not at present possible to use our theoretical calculations to draw comparisons between the $\{Fe^{II}(CN)_5\}^{3-}$ and $\{Ru^{II}(NH_3)_5\}^{2+}$ complexes because they have been calculated at different levels of theory. Meaningful comparisons would require a computational method that is suitable for both types of compound (the LanL2DZ basis set is inadequate for anions and 6-311+G* is not defined for ruthenium).

(42) Shin, Y.-g. K.; Brunschwig, B. S.; Creutz, C.; Sutin, N. *J. Am. Chem. Soc.* **1995**, *117*, 8668−8669.

Conclusions

We have synthesized and characterized a family of MLCT chromophores based on electron-donating $\{Fe^{II}(CN)_5\}^{3-}$ centers. HRS measurements at 1064 nm show that these complexes have relatively large static first hyperpolarizabilities, β_0, which increase markedly on moving from aqueous to methanol solutions. This solvent dependence of NLO responses can be traced to large red-shifts in the MLCT transitions, which are shown by cyclic voltammetry to be attributable to destabilization of the Fe-based HOMOs *and* simultaneous stabilization of the acceptor ligand-based LUMOs. Stark spectroscopic studies in glycerol−water (50:50 vol %) glasses at 77 K confirm and rationalize the large β_0 values according to the two-state model. Acidification of solutions of the dipolar Fe^{II} complexes leads to large, reversible blue-shifts in their MLCT bands due to protonation of the cyanide ligands. These increases in MLCT energies are accompanied by several-fold decreases in the β_0 responses, as shown via both HRS and Stark experiments, demonstrating a novel approach to protic-switching of molecular NLO properties. TD-DFT and FF calculations using a PCM yield relatively good agreement with the experimental results and confirm (but overestimate) the large decrease in NLO response on protonation. The available physical data permit detailed comparisons with previously reported chromophores with $\{Ru^{II}(NH_3)_5\}^{2+}$ electron donor centers. The Stark-derived β_0 values are generally larger for the Ru^{II} complexes than for their Fe^{II} analogues due to lower E_{max} and higher μ_{12} values which more than offset the decreases of $\Delta\mu_{12}$ in the Ru^{II} complexes. This observation agrees with the HRS data in water, but the HRS data in methanol show that the Fe^{II} complexes have the larger β_0 responses. The more pronounced solvatochromism of the Fe^{II} complexes means that their NLO performance can surpass that of their $\{Ru^{II}(NH_3)_5\}^{2+}$ counterparts upon changing the solvent medium.

Acknowledgment. We thank the EPSRC for support (Grant No. GR/R54293 and a Ph.D. studentship) and also the Flemish Fund for Scientific Research (FWO-V, Grant No. G.0297.04), the University of Leuven (GOA/2006/3), the Belgian Government (IUAP P5/3), MCyT-FEDER (BQU2005-01368) and Gobierno de Aragon-Fondo Social Europeo (E39). I.A. acknowledges a fellowship from the FWO-V.

Supporting Information Available: Tables S1−S3; Figures S1−S3; Cartesian coordinates of theoretically optimized geometries for the anionic complexes in **1** and **5** and for the complexes in **1**H, **1**H_2 and **1**H_5; complete refs 3d, 3j, 24, and 38b (PDF). This material is available free of charge via the Internet at http://pubs.acs.org.

JA063449M